Exploring the interactive TX-molecules: Applicable 4-cyclopentene-1,3-dione and 2-nitroimidazole structure for drug design

2020

大倉　一人

CONTENTS

Chapter 1.   Preface

In structural design for biological active molecule, the movement of the designed compound should be considered.   Molecular motion is caused by stretching and rotation of interatomic bonds.   It is also important to observe the three-dimensional structure into planes. For example, when the plane A and the plane B are coupled with a single bond, the positional relationship between the planes A and B changes due to their rotation (Figure 1-1).   The dihedral angle, which is formed by plane angle between the triangle a-b-c and the triangle b-c-d, is very convenient parameter (Figure 1-1 and Figure 1-2).   In a case as the side chains R1 and R2 are bonded to planes A and B, the hydrophobicity of the whole molecule affected by structural change at the side chain R1 and R2.   The molecular hydrophobicity greatly affects the interaction ability with the target structure, then the side chain (*e.g.* R1 and R2) movement and the dihedral angle (*e.g.* plane angle between a-b-c and b-c-d) change is an important factor.
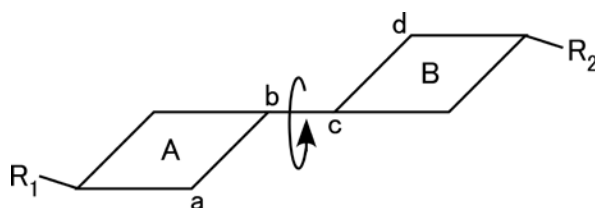
Figure 1-1.   Relationship between plane A and B.
Triangle a-b-c and b-c-d formed dihedral angle, and positional relationship
of plane A and B is changed by dihedral angle situation.
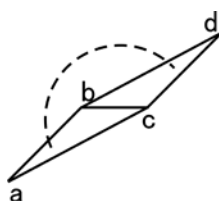
Figure 1-2.   Dihedral angle between two triangles.
Triangle a-b-c and b-c-d formed dihedral angle.

In the interactive analysis between protein and ligand, the structural feature of ligand bindable pockets in the protein molecule should be considered.   The ligand binding pattern can be verified by simulating the ligand invasion mode into the cavity of protein molecule. The hydrophobicity of the interacting site between the ligand and target protein can be inferred from the solvation free energy (dGW), which is one of the molecular orbital parameter that reflects their conformation (Ohkura K. *et al.* (1999)).   The lower dGW value means higher hydrophobicity.   In addition, the stability of the interacting molecules can be evaluated from the heat formation energies when dGWs are calculated.

The compounds examined in the present study include five-membered ring components such as 1,3-cyclopentenedione and 2-nitroimidazole.   These ring structure can serve as a place for transferring electrons, the molecular features can be changed by introducing various functional groups, and as a result, various functions are easily provided. Based on these facts, the effects of the molecular parameters (*e.g.* stability, stereo-hydrophobicity, flexibility) of designed molecules on the interactive ability and biological activity (*e.g.* radiosensitizing ability, enzyme inhibition) were explored.

Chapter 2.   Molecular features of 2-hydroxyarylidene-4-cyclopentene-1,3-dione scaffold TX-1123 derivatives

2-1.   Background

Selection of a scaffolding structure is very important for molecular design of a compact and efficient radiation sensitizer.   So far, we have been designed and synthesized several low molecular radiosensitizing compounds, and examined the usefulness of units with 1,3-cyclopentenedione structure.   In particular, TX-1123 benefits for its low cytotoxicity and high radiosensitizing ability, and the relationship between structure and function of TX-1123 derivatives was discussed.

Protein kinase runaway is associated with various diseases, and the development of compounds that regulate protein tyrosine kinases can provide clues for the diseases treatment. There are various types of tyrosine kinases such as cyclin-dependent (cd) kinase2 (Blume-Jensen P. *et al.* (2001), Higashi H. *et al.* (1996), Jeffrey P.D. *et al.* (1995)) and proto-oncogene tyrosine-protein (Src) kinase (Blume-Jensen P. *et al.* (2001), Hubbard S.R. *et al.* (2000), Levitzki A. (1992), Richardson JM. *et al.* (1987), Ullrich A. *et al.* (1990)), and they are involved in maintaining biological functions.   In the present report, Src kinase inhibitory function of designed low molecular weight 1,3-cyclopentenedione compounds were discussed.

The TX series containing 1,3-cyclopentenedione structure was designed and synthesized (Hori H. *et al.* (2002)).   These compounds have a common structure with Tyrphostin AG17.   The SF6847 (an alternate name for Tyrphostin AG17) was shown to act as an uncoupler of oxidative phosphorylation in isolated rat liver and heart mitochondria (Terada H. *et al.* (1988)).   Two cyano groups of Tyrphostin AG17 molecule are in the same

plane.   In TX-1123, TX-1918, TX-1925, TX-1926 molecule, by introducing 1,3-cyclopentendione ring instead of two cyano groups, the two planes of benzene ring and cyclopentene ring were moving independently of each other.   In addition, TX-1927 was designed and synthesized by introducing a methyl group into the phenolic hydroxyl group of Tyrphostin AG17 and modifying the reactivity (Hori H. *et al.* (2002)).   The TX-1123 derivatives were compared for their ability to inhibit Srk kinase and their molecular features were evaluated.   Interactive analysis between TX-1123 derivatives and Src kinase had been performed, and explored more efficient kinase control.

Cyclooxygenase (COX) is involved in the production of prostaglandins, and the prostaglandin cascade is a target for drug therapy.   In COX targeting compound design, molecular features of COX1 and COX2 should be considered.   COX-1 is a constitutive enzyme that is widely distributed in tissues throughout the body and expressed in the endoplasmic reticulum (Vane J.R. *et al.* (1998)).   COX-1 presents in a constant amount in the cell and can be induced by a specific stimulus.   On the other hand, COX-2 is constitutively expressed in the brain and kidney, but is usually lower expressed in other tissues, and its expression is induced in inflammatory tissues.   Side effects such as gastric ulcers are often a problem with COX1 inhibitors.   COX2 selective inhibitors have a low risk of digestive disorders (Fitzpatrick F.A. (2004)).   The inhibitory potency of TX-1123 derivatives to COX1 and COX2 was compared and verified.   Interactive analysis of TX-1123 derivatives with COX1 or COX2 were performed using simulation technique. Through these things, capability of TX-1123 derivatives as anti-inflammatory drugs were discussed.   The potential of TX-1123 derivatives as anti-inflammatory drug have been explored.

2-2. Antitumor 2-hydroxyarylidene-4-cyclopentene-1,3-dione as protein tyrosine kinase inhibitor: Interaction analysis of TX-1123 derivatives with Src kinase

2-2-1. Introduction

Protein tyrosine kinases (PTKs) are members of a family of oncoproteins and proto-oncoproteins, and they play major roles in the signal transduction during normal cell division, terminal cell differentiation, and apoptosis (Ullrich A. *et al.* (1990), Richardson J.M. *et al.* (1987), Levitzki A. (1992), Blume-Jensen P. *et al.* (2001), Hubbard S.R. *et al.* (2000)). PTK activity is associated with proliferative disorder such as cancer, and PTK inhibitor was developed as potential therapeutic agent (Levitzki A. *et al.* (1995), Umezawa H. *et al.* (1986), Yaish P. *et al.* (1988)). Tyrphostins were examined as the low molecular weight PTK inhibitors designed to compete with substrate rather than ATP molecule (Gazit A. *et al.* (1989), Levitzki A. (1990)).

The insulin suppressive effect of tyrphostin AG17 in rat white adipocytes was reported (Ohkura K. *et al.* (2001)). Tyrphostin AG17 induced the apoptosis and inhibited cyclin-dependent kinase 2 (cdk2) activity through a mechanism that purportedly does not involve reductions in cellular ATP level (Palumbo G.A. *et al.* (1997)). Based on potential mechanisms underlying the antiproliferative effects of tyrphostin AG17, it is important that SF6847 (an alternate name for Tyrphostin AG17) has been shown to act as an uncoupler of oxidative phosphorylation in isolated rat liver and heart mitochondria (Terada H. *et al.* (1988)). Lower mitochondrial toxicity of tyrphostin AG17 analog, such as TX-1123, was previously described (Hori H. *et al.* (2002)). In the present study, kinase-inhibitory activities of TX-1123 derivatives (Figure 2-1) were examined, and analyzed the binding profiles of these TX-1123 family members using docking simulation.
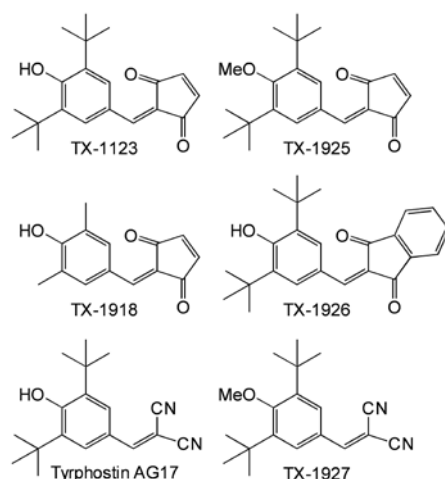
Figure 2-1.   Structure of TX-1123 derivatives and tyrphostin AG17

2-2-2.   Materials and Methods

Inhibition of proto-oncogene tyrosine-protein (Src) kinase activity.

The PTK inhibitory effect of synthesized compounds were summarized from our previous report (Hori H. *et al.* (2002)).   The v-*src* transformed NIH3T3 cells were incubated for 10 min on ice in hypotonic buffer (1 mM Hepes (pH 7.0), 4.5 mM MgCl$_2$, and 25 µg/mL protease inhibitor (antipain, leupeptin, pepstatin A)).   Following an increase of HEPES to 20 mM, homogenate was centrifuged at 500 g for 5 min.   To this supernatant, addition was made to give a final concentration of 20 mM HEPES (pH 7.4), 10 mM MgCl$_2$, 0.1 mM Na$_3$VO$_4$, 10 mM β-glycerophosphate, 1 mM NaF, 2.5 mg/mL protein, 1 µM phorbol myristate 13-acetate and 20 µM cAMP.   Kinase reaction was initiated by addition of [γ-^{32}P]ATP (12.5 µM, 10 µCi), and solution was incubated for 15 min at 25 ^{o}C.   Phosphorylated proteins were separated by SDS-PAGE (9% gel).   Results were visualized by autoradiography or Bio-image Analyzer BAS 2000 (Fuji Film Co., Tokyo, Japan).   From the enzyme activity (as a percentage to the control) as a function of drug concentration, the half maximal-inhibitory

concentration (IC_{50}) values were estimated as the index of enzyme inhibition of designed compounds.

Analysis of interaction of TX-1123 derivatives with Src kinase.

The Src kinase structure was obtained from a protein data bank (PDB ID=2SRC). Interactive analysis between TX-1123 derivatives and Src kinase was examined by the molecular mechanics (MM) and molecular dynamics (MD) simulation technique using insightII discover under consistent valence force field (Accelrys Inc., San Diego, CA, USA) and molegro virtual docker (CLC bio, Aarhus, Denmark), as previously described (Kawaguchi Y. *et al.* (2013), Ohkura K. *et al.* (2012)).

2-2-3.   Results

Inhibition of Src kinase activity by TX-1123 derivatives.

TX-1123 exhibited the most potent inhibition of Src kinase activity among the tested compounds, and the IC_{50} value was 2.2 μM (Table 2-I).   Src kinase inhibition was suppressed by the addition of a methoxy group to TX-1123 molecule, and the IC_{50} value of the synthesizing derivative TX-1925 was 3.1 μM.   The replacement of two sterically-bulky *tert*-butyl groups in TX-1123 by two methyl groups reduced its inhibitory activity, with an IC_{50} of the resulting derivative TX-1918 was 4.4 μM.   The addition of a benzene ring to the cyclopentenedione site of TX-1123 also reduced the inhibitory activity (TX-1926: $IC_{50} > 27$ μM).   The mitochondrial uncoupling drug tyrphostin AG17 exhibited weak inhibition of Src kinase activity ($IC_{50} > 350$ μM).   Methoxy tyrphostin AG17 (TX-1927) had a similarly high IC_{50} value (> 340 μM).

Table 2-I.   Protein Src kinase inhibitory activities and interaction energy of TX-1123 derivatives.

Drugs	IC$_{50}$ (μM)	Total energy (kcal/mol)
TX-1123	2.2	−115.808
TX-1925	3.1	−106.957
TX-1918	4.4	−102.254
TX-1926	>27	−116.078
TX-1927	>340	−98.813
Tyrphostin AG17*	>350	−98.821

*IC$_{50}$ value of tyrphostin AG17 was indicated 75% inhibition concentration.

Ligand-bindable pockets in Src kinase molecule.

The Src kinase (protein data bank ID = 2SRC) molecule flexibly moved during the MM-MD simulation period, and three major ligand-bindable pockets were detected in the Src kinase molecule (Figure 2-2, pocket A-C).   The large bindable pocket A spread at the center of the Src kinase molecule.   Pocket B and pocket C existed at a position shifted from the center of the Src kinase molecule.   The bindable pocket B was identified as the ligand (c-AMP)-binding site of Src kinase by interactive analysis between Src kinase and c-AMP (Figure 2-3A), and consistent with X-ray crystallographic data (2SRC).   Binding of TX-1123 derivatives were detected at pocket B in the present ligand-binding simulation.
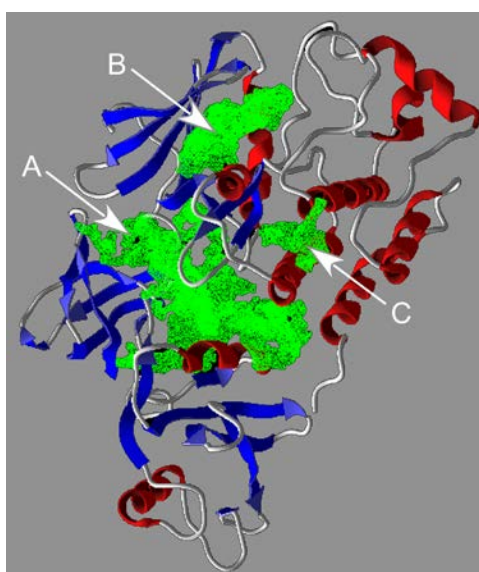
Figure 2-2.   Binding pockets of the Src kinase molecule.
Three ligand-bindable pockets (green clouds: A-C) were detected.

Binding features of TX-1123 derivatives.

TX-1123 bound at pocket B (arrow in Figure 2-3B), and the binding position was shifted more to the right than that of c-AMP (arrow in Figure 2-3A). An interaction was observed between the phenolic hydroxyl group of TX-1123 and the phenolic hydroxyl group of Tyr[416] of Src kinase molecule (Figure 2-3C), and the total interaction energy was -115.808 kcal/mol (Table 2-I).
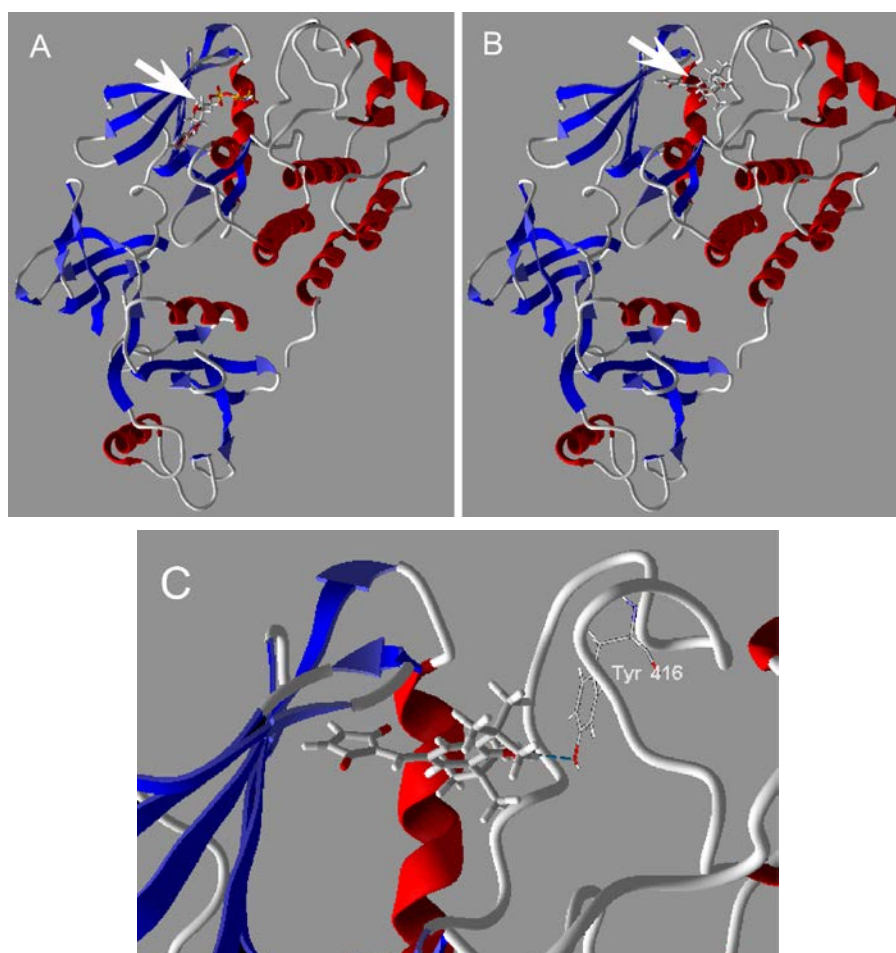
Figure 2-3. Binding profile of ligands to Src kinase.
A: c-AMP (arrow) fitted in pocket B (see Figure 2-2) of Src kinase.
B: TX-1123 (arrow) fitted in pocket B of Src kinase.
C: The phenolic hydroxy group of TX-1123 interacted with Tyr[416] of Src kinase.

TX-1925 and TX-1918 exhibited the Src kinase inhibition similarly to TX-1123 (Table 2-I), and bound at the pocket B. The binding position of TX-1925 to Src kinase was shifted downward from that of c-AMP (arrow in Figure 2-4A), and the total interaction energy was -106.957 kcal/mol. The binding position of TX-1918 was also shifted downward from that of c-AMP (arrow in Figure 2-4B), and the total interaction energy was -102.254 kcal/mol. TX-1918 interacted with the phenolic hydroxyl group of Phe[405] of Src kinase through its own phenolic hydroxyl group (Figure 2-4C).
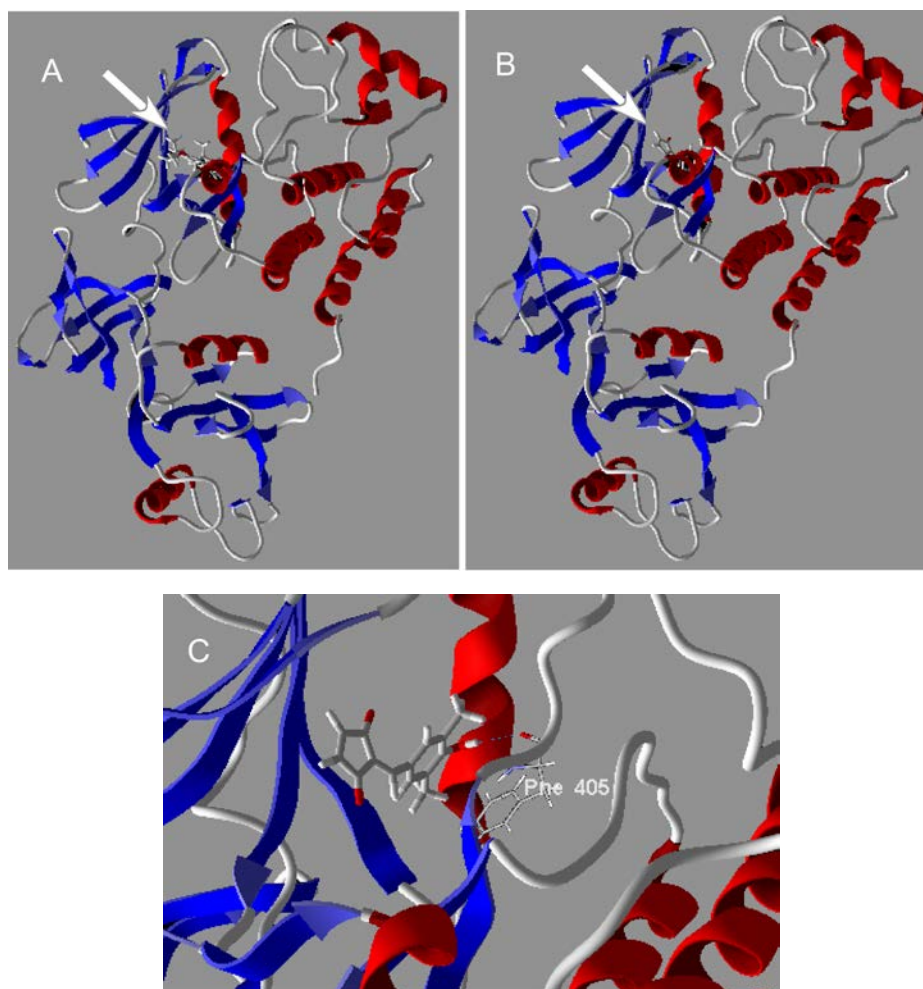
Figure 2-4.   Interaction profiles of TX-1123 derivatives with Src kinase.
TX-1925 (A), TX-1918 (B) fitted in Src kinase pocket B.
TX-1918 interacted with the phenolic hydroxyl group of Phe[405] in Src kinase through its own phenolic hydroxyl group (C).

The binding position of TX-1926 was near to that of c-AMP (arrow in Figure 2-4D). TX-1926 showed good binding energy (-116.078 kcal/mol) similar to that for TX-1123, whereas its Src kinase inhibitory activity was weaker than those of TX-1123, TX-1925, and TX-1918 (Table 2-I). Binding position of TX-1927 was almost the same as that of TX-1123 (arrow in Figure 2-4E). TX-1927 interacted with the phenolic hydroxyl group of Tyr[416] and amino group of Gly[276] of Src kinase through its own phenolic hydroxyl group and cyano group, respectively (Figure 2-4F). The binding energy (-98.813 kcal/mol) and Src kinase inhibition of TX-1927 ($IC_{50} > 340$ μM) were significantly weaker than those of TX-1123.
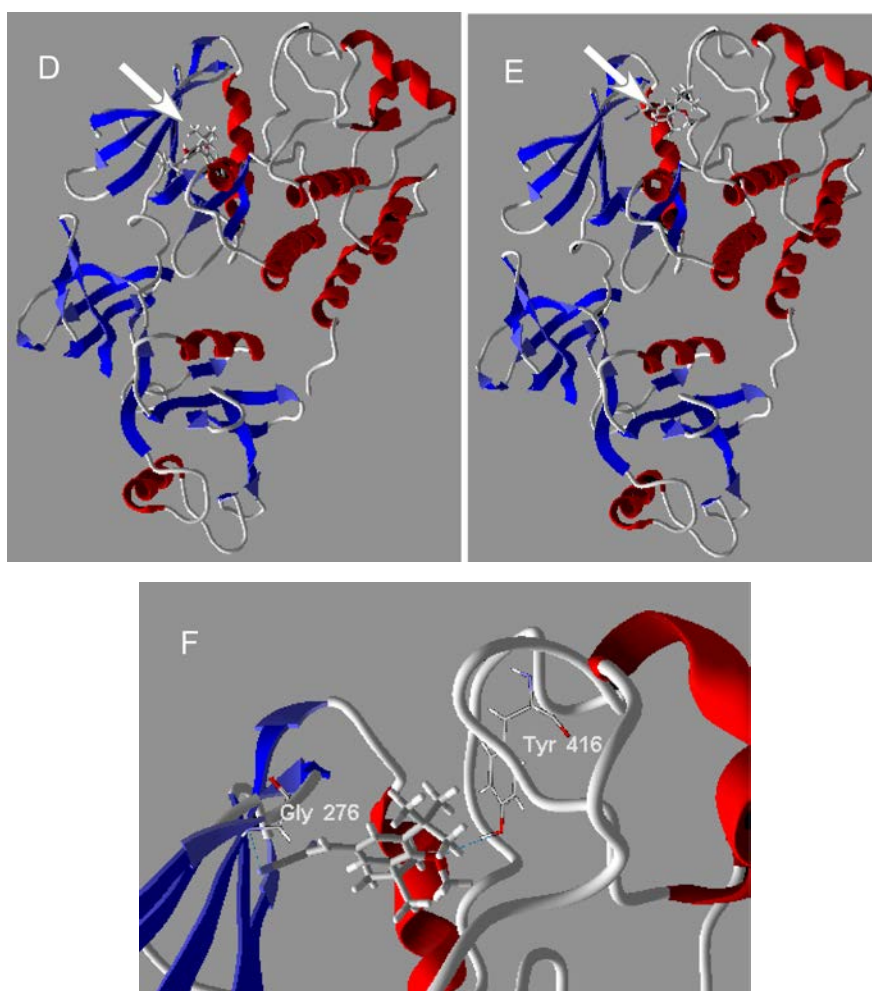
Figure 2-4. Interaction profiles of TX-1123 derivatives with Src kinase.
TX-1926 (D) and TX-1927 (E) fitted in Src kinase pocket B.
TX-1927 interacted with phenolic hydroxyl group of Tyr[416] and amino group of Gly[276] of Src kinase through its own phenolic hydroxyl group and cyano group, respectively (F).

13

Tyrphostin AG17 bound to a different Src kinase molecule site from the TX-1123 derivatives (arrow in Figure 2-4G), and the phenolic hydroxyl group of Tyr[90] interacted with cyano group of tyrphostin AG17. The two carboxyl groups of Tyr[149] and Gln[144] of Src kinase interacted with the phenolic hydroxyl group of tyrphostin AG17 (Figure 2-4H). The binding energy of tyrphostin AG17 (-98.821 kcal/mol) was equivalent to that of TX-1927.
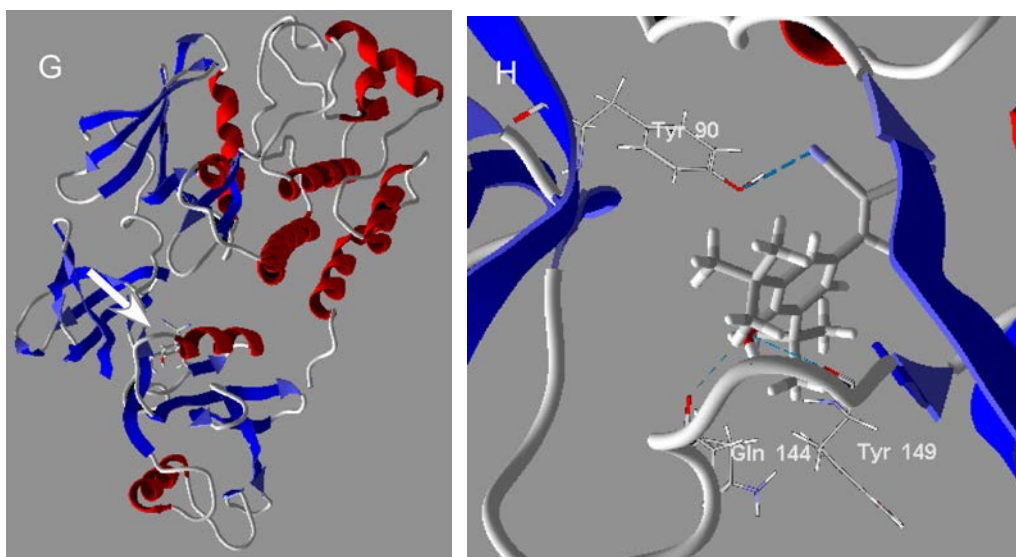
Figure 2-4.   Interaction profiles of TX-1123 derivatives with Src kinase.
Tyrphostin AG17 fitted in a different Src kinase site (pocket A) from TX-1123 derivatives (G). The cyano group of tyrphostin AG17 interacted with the hydroxyl group of Src kinase Tyr[90], and the phenolic hydroxyl group of tyrphostin AG17 interacted with two carboxyl groups of Src kinase Tyr[149] and Gln[144] (H).

2-2-4. Discussion

The 2-Arylidine-4-cyclopentene-1,3-diones, which were unique soft acid-type electrophilic cyclopentene-1,3-dione moieties, had been reported to be antitumor compounds (Inayama S. *et al.* (1976)). Non-nitro radiosensitizing hypoxic cytotoxin 2-hydroxyarylidene-4-cyclopentene-1,3-diones such as KIH-200, KIH-201, and KIH-202 had been developed (Hori H. *et al.* (1987)). These synthesized KIH members were found to be potent inhibitors of phosphate transport in mitochondria inner membrane (Koike H. *et al.* (1988)). The hydroxy-benzylidene-cyclopentenedione compound was developed as a phenolic enhancer of chemiluminescence, and KIH-201 was the potent enhancer of the luminol-hydrogen-horseradish peroxidase peroxide reaction (Hori H. *et al.* (1994)). These cyclopentenedione moieties instead of malononitrile moieties found in the tyrphostin AG17 molecule were expected to result in reduced the mitochondrial toxicity. Tyrphostin AG17 exhibited potent mitochondrial cytotoxicity, and the mitochondrial uncoupling activity (C_{max} = 0.02 µM, V_{max} = 270 nanoatomO/mg/min) and the ATP synthesis inhibition (IC_{50} = 0.0035 µM) were observed (Hori H. *et al.* (2002)). TX-1123 was a designed tyrphostin AG17 analog, and exhibited lower mitochondrial cytotoxicity (uncoupling activity (C_{max} = 2 µM, V_{max} = 260 nanoatom O/mg/min) and the ATP synthesis inhibition (IC_{50} = 5 µM)).

Different binding features of TX-1123 derivatives to the Src kinase molecule compared with those of c-AMP binding were observed in a binding simulation. In general, native protein kinase was found to exist with a solvent molecule (*e.g.* water), and some solvent molecules were included in the kinase pocket (Otto R. *et al.* (2012)). The X-ray crystallographic data for c-AMP interaction with Src kinase presents the momentary positional relationship each other, and reflects neither molecular fluctuation nor interaction with solvent (Helliwell J.R. (1992), Gruner, S.M. (1994), Rossmann M.G. *et al.* (1992), Brunger A.T. *et al.* (1993)). Molecular docking simulation was considered appropriate

because the verified interactive analysis between a ligand (*e.g.* TX-1123 derivatives) and protein (*e.g.* Src kinase) was performed with various solvents.

TX-1123 bound to a near site of c-AMP-binding pocket in Src kinase molecule, and inhibited kinase activity. Phenolic hydroxy group of TX-1123 interacted with Src kinase Tyr[416], and methylation of this TX-1123 phenolic hydroxy group (*e.g.* TX-1925) also inhibited Src kinase activity (Table 2-I). In TX-1918 molecule without the bulky *tert*-butyl groups of TX-1123, the mobility of the phenolic hydroxy group increased, and indicating reaction features different from those of TX-1123 by an interaction with Phe[405] in Src kinase.

The flexibility of TX-1926 was altered by the addition of a six-membered ring to the 1,3-cyclopentenedion site, and the anti-kinase activity decreased. In tyrphostin AG17, the 1,3-cyclopentenedione site was substituted for two cyano groups, and the molecular frame was altered. The structural features of tyrphostin AG17 were altered more than those of TX-1123, and not only the phenolic hydroxy group, but also the cyano groups interacted with the Src kinase molecule. TX-1927 had a molecular backbone to similar that of tyrphostin AG17, and the reactivity with Src kinase was not affected by the methylation of phenolic hydroxy group. This result did not contradict Src kinase inhibitory activity not being significantly influenced by the methylation of phenolic group in TX-1925 molecule.

It appears to be possible to develop drugs with anticancer activity based on the control of protein kinase function, even with small molecules such as TX-1123 derivatives, by using a interactive simulation between tested compounds and target protein kinase.

2-3. Interaction between TX-1123 and cyclo-oxygenase: Design of COX2 selective TX analogs

2-3-1. Introduction

Non-steroidal anti-inflammatory drugs (NSAIDs) are widely used in clinical therapy. The anti-inflammatory effect of NSAIDs are attributable to reductions of the formation of prostaglandins (PGs) (Steinmeyer J. (2000), Suleyman H. *et al.* (2007)). This ability is associated with the inhibition of cyclo-oxygenase (COX) activity, which converts arachidonic acid to PGH$_2$. So far, two isoforms of COX (*i.e.* COX1 and COX2) have been identified. COX1 is expressed constitutively and is the housekeeping enzyme responsible for physiological activity of PG. COX2 is expressed under inflammatory condition, and is responsible for pathological PG that produce pain and fever (Baek S.J. *et al.* (2006), Watanabe T. *et al.* (2011), Wang X. *et al.* (2011)). Side effects such as gastric ulcers are often a problem with COX1 inhibitors. COX2 selective inhibitors (*e.g.* celecoxib) have a low risk of digestive disorders (Fitzpatrick F.A. (2004), Crofford L.J. (1997)). The inhibitory potency of TX-1123 derivatives to COX1 and COX2 was compared and verified. Interactive analysis of TX-1123 derivatives with COX1 or COX2 were performed using molecular simulation technique.

Tyrphostin AG17 induced apoptosis and inhibited cyclin-dependent kinase 2 activity through a mechanism that purportedly did not involve reductions in cellular ATP level (Palumbo G.A. *et al.* (1997)). Tyrphostin AG17 has been shown to act as an uncoupler of oxidative phosphorylation in isolated rat liver and heart mitochondria (Terada H. *et al.* (1988)). Tyrphostin AG17 was shown to suppress the effects of insulin in rat adipocytes (Ohkura K. *et al.* (2001)). Designed tyrphostin AG17 analogs have a

17

2-hydroxyarylidene-4-cyclopentene-1,3-dione structure (Figure 2-1). TX-1123 has been shown to possess useful features (*e.g.* strong Src kinase inhibitory activity and weak mitochondrial cytotoxicity) (Hori H. *et al.* (2002), Ohkura K. *et al.* (2016)). In the present study, the COX-inhibitory activities of TX-1123 derivatives were examined, and analyzed the binding profiles of TX-1123 derivatives with COXs using docking simulations.

2-3-2.   Materials and Methods

Assay for COX inhibition.

COX1 and COX2 proteins were isolated from ram seminal vesicles and sheep placenta, and the inhibitory effect of tested compounds on these COXs were examined as previously described (Futaki N. *et al.* (1994)). Mixture of Tris-HCl buffer 10 µl (100 mM), hematin 10 µl (1 µM), phenol 10 µl (2 mM), and 50 µl of distilled water was added to 10 µl of test materials dissolved in 1% DMSO. Then 200 U of COX-1 or COX-2 was added to mixture. Reaction medium was preincubated with each of extract samples for 2 min at 37 $^{\circ}$C, and 2 µl of 51.4 µM [1-^{14}C] arachidonic acid was added and incubated for 2 min at 37 $^{\circ}$C. After terminating reaction in an ice bath, 0.4 ml of *n*-hexane/ethyl acetate (2 : 1, v/v) was added to mixtures and centrifuged at 2000 g for 1 min. Amount of radioactivity in supernatant was measured using a scintillation counter. COX1- and COX2-inhibitory effect of celecoxib were examined by COX1-mediated PGE2 production in human lymphoma cells (half maximal-inhibitory concentration: IC$_{50}$) and COX2-mediated PGE$_2$ production in human dermal fibroblasts (IC$_{50}$), respectively (Yoshino T. *et al.* (2005)).

Interactive analysis of TX-1123 with COXs.

The X-ray crystallographic data sets of COX1 (protein data bank ID = 1PGG) and

COX2 (ID = 3LN1) were used for molecular interactive simulation.   The interactive analysis between TX-1123 derivatives and COXs were examined by molecular simulation technique (Molecular Mechanics (MM)-Molecular Dynamics (MD)) using InsightII Discover under consistent valence force field (Accelrys Inc., San Diego, CA, USA) and Molegro Virtual Docker (CLC bio, Aarhus, Denmark) as previously described (Ohkura K. *et al.* (2016), Kawaguchi Y. *et al.* (2013), Ohkura K. *et al.* (2012)).   The ligand-bindable pocket and the electrostatic potential (ESP) fields of COXs were examined using Molegro Virtual Docker.

2-3-3.   Results

Effects of TX-1123 derivatives on COX activity.

TX-1123 exhibited COX1-inhibitory activity, and the half maximal inhibitory concentration (IC_{50}) was 1.57×10^{-5} M (Table 2-II).   The COX2-inhibitory activity of TX-1123 was potent ($IC_{50} = 1.16 \times 10^{-6}$ M).   The ratio of COX1/COX2 inhibition ($R_{C1/C2}$) of TX-1123 was 13.5. $R_{C1/C2}$ is an index of COX2 selectivity.   The COX2-inhibitory effect of TX-1123 was higher than that of COX1-inhibitory effect.   TX-1925 exhibited inhibition toward COX1 ($IC_{50} = 4.77 \times 10^{-5}$ M) and COX2 ($IC_{50} = 1.03 \times 10^{-5}$ M), and the $R_{C1/C2}$ value was 4.63. $R_{C1/C2}$ values of TX-1918, TX-1926, and TX-1934 were less than 1.0 (0.11–0.77), and these TX-1123 derivatives were not selective for COX2.   Tyrphostin AG17 weakly inhibited COX1 (2.29×10^{-3} M) and COX2 (3.23×10^{-4} M), and IC_{50} values of 10-fold or greater than those of the TX-1123 derivatives.

The COX-inhibitory activity of celecoxib, which is a well known COX2-selective drug, was demonstrated using the production of PGE_2 in human lymphoma cells, and the IC_{50} values (2.80×10^{-6} M (COX1) and 9.10×10^{-8} M (COX2)) were summarized from previous report (Yoshino T. *et al.* (2005)).

Table 2-II.   Effect of TX series molecules on COX1 and COX2 activity.

| | IC$_{50}$ (M) | | |
	COX1	COX2	R$_{C1/C2}$
TX-1123	1.57 x 10^{-5}	1.16 x 10^{-6}	13.5
TX-1925	4.77 x 10^{-5}	1.03 x 10^{-5}	4.63
TX-1918	7.35 x 10^{-5}	6.56 x 10^{-4}	0.11
TX-1926	6.84 x 10^{-6}	8.86 x 10^{-6}	0.77
TX-1934	1.82 x 10^{-4}	8.15 x 10^{-4}	0.22
Tyrphostin AG17	2.29 x 10^{-3}	3.23 x 10^{-4}	7.09
Celecoxib	2.80 x 10^{-6}	9.10 x 10^{-8}	30.8
Indomethacin	3.10 x 10^{-6}	1.50 x 10^{-4}	0.02

IC$_{50}$: Half maximal-inhibitory concentration;   R$_{C1/C2}$: inhibition ratio of COX1/COX2 as determined by the ratio of IC$_{50}$ for COX1 and COX2.

Ligand-bindable pockets in COX2 molecule.

The COX2 and COX1 molecules flexibly moved during MM-MD simulation under consistent valence force field.   Three major ligand-bindable pockets (A - C) were observed in the COX2 molecule (green clouds in Figure 2-5A).   Similar three ligand-bindable pockets of COX1 molecule were also detected as well as COX2 (Figure 2-5B).
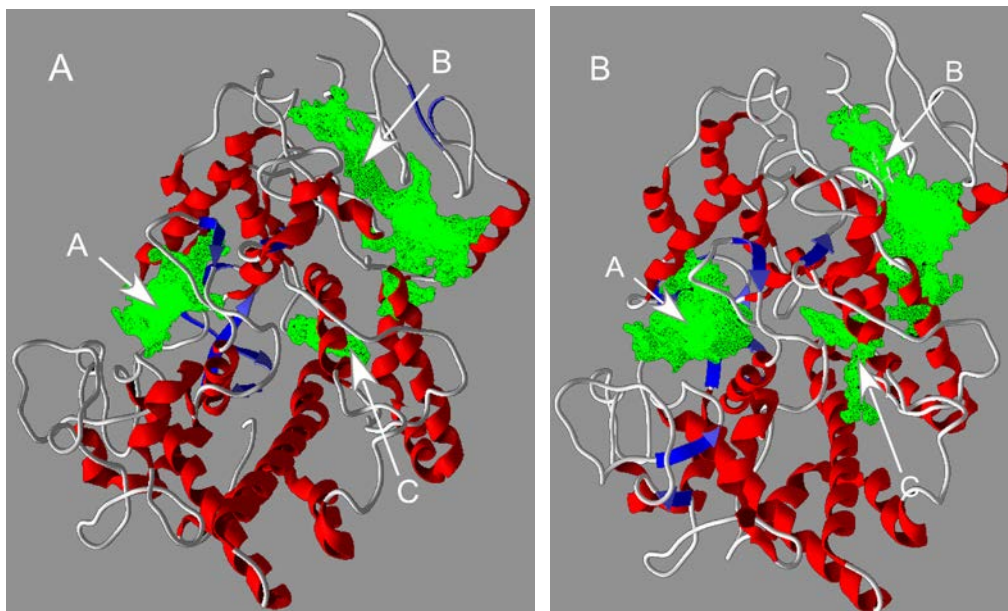
Figure 2-5.   Ligand-bindable pockets of cyclo-oxygenase molecule.
Three ligand-bindable pockets (green clouds: A - C) of COX2 (A) and COX1 (B) were detected.

Interaction between TX-1123 and COXs.

TX-1123 bound at COX2 pocket B (arrow in Figure 2-6A), and the oxygen atom of the 4-cyclopentene-1,3-dione region of TX-1123 interacted with Cys^{26} (nitrogen atom) and Gln^{447} (the nitrogen atom of amide group) (Figure 2-6B). COX2-selective celecoxib bound at pocket C (arrow in Figure 2-6C), and the oxygen atom of sulfonamide group in celecoxib molecule (green circle in Figure 2-8) interacted with both Ile^{503} (nitrogen atom) and Phe^{504} (nitrogen atom) (Figure 2-6D). The nitrogen atom of sulfonamide group of celecoxib (green circle in Figure 2-8) interacted with Phe^{504} (the oxygen atom of hydroxy group).
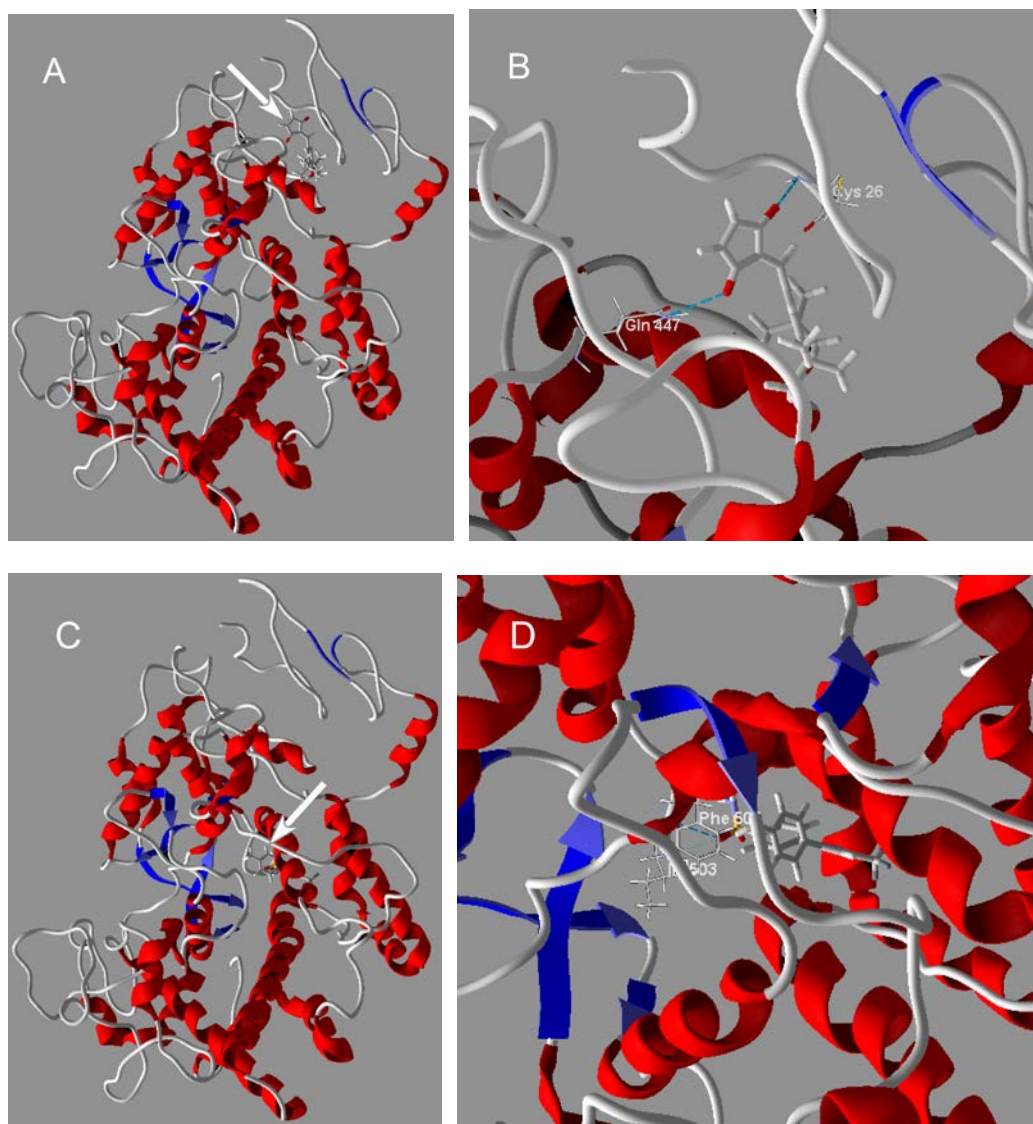
Figure 2-6.   Binding profiles of ligands to COX2.
A: TX-1123 bound to pocket B (Figure 2-5A) of COX2.   B: Cyclopentene-1,3-dione of TX-1123 interacted with Cys^{26} and Gln^{447} of COX2.   C: Celecoxib bound to pocket C of COX2.   D: Sulfonamide group of celecoxib interacted with Ile^{503} and Phe^{504} of COX2.

TX-1123 bound COX1 pocket B, and the oxygen atom of 4-cyclopentene-1,3-dione group of TX-1123 interacted with Cys^{41} (nitrogen atom) and Gln^{461} (the nitrogen atom of amide group) (Figure 2-7A and 2-7B). The oxygen atom of TX-1123 phenolic group interacted with COX1 Arg^{469} (the nitrogen atom of side chain). Indomethacin bound to COX1 pocket C (arrow in Figure 2-7C), and the carboxyl group oxygen atom of indomethacin (blue circle in Figure 2-8) interacted with COX1 Tyr^{355} (phenolic hydroxyl group) (Figure 2-7D). Indomethacin also bound to COX2 pocket A, and methoxy group at indole skeleton (oxygen atom) interacted with Thr^{198}, and carboxyl group (oxygen atom) interacted with His^{372} (B) (Figure 2-9).
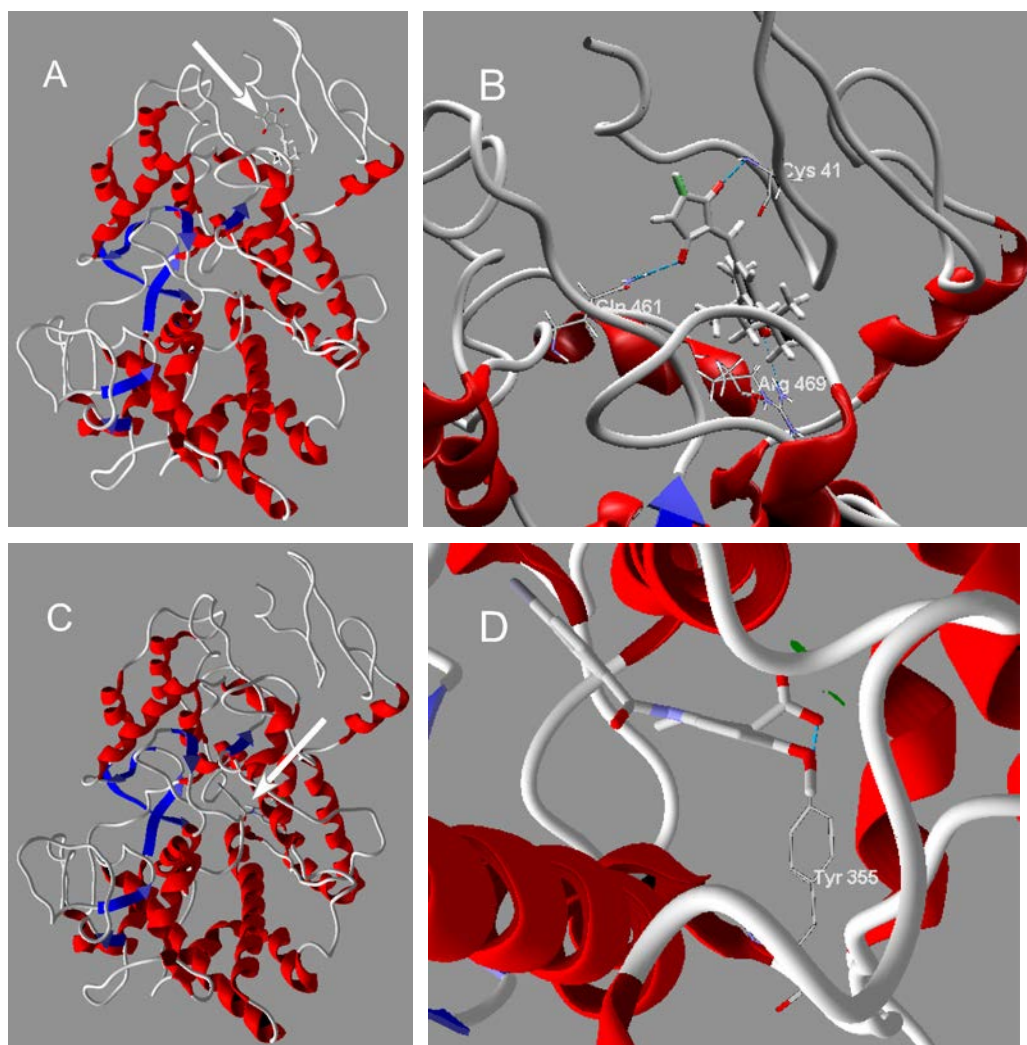
Figure 2-7.   Interaction profiles of ligands to COX1.
A: TX-1123 bound to COX1 pocket B.   B: Cyclopentene-1,3-dione of TX-1123 interacted with Cys^{41} and Gln^{461} of COX1.   Phenolic group of TX-1123 interacted with Arg^{469} of COX1.   C: Indomethacin bound to COX1 pocket C.   D: Carboxyl group oxygen atom of indomethacin interacted with COX1 Tyr^{355} (phenolic hydroxyl group)
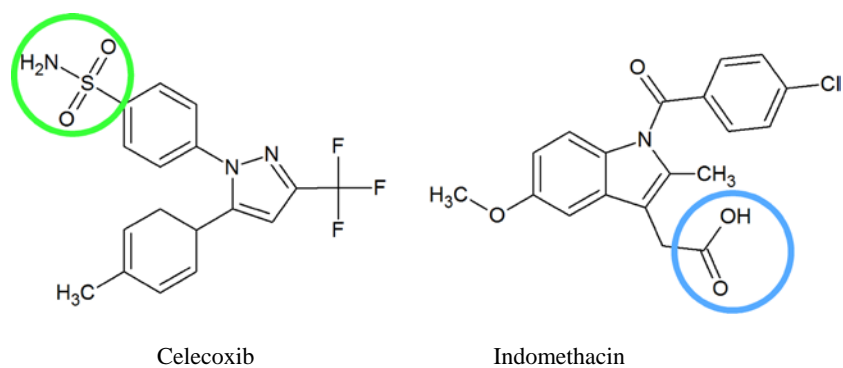
Figure 2-8. Molecular structure of celecoxib and indomethacin.
Structures of COX2 selective inhibitor (celecoxib) and COX1 selective inhibitor (indomethacin).
Interactive sulfonamide group of celecoxib (green circle) and carboxyl group indomethacin
(blue circle) are shown.
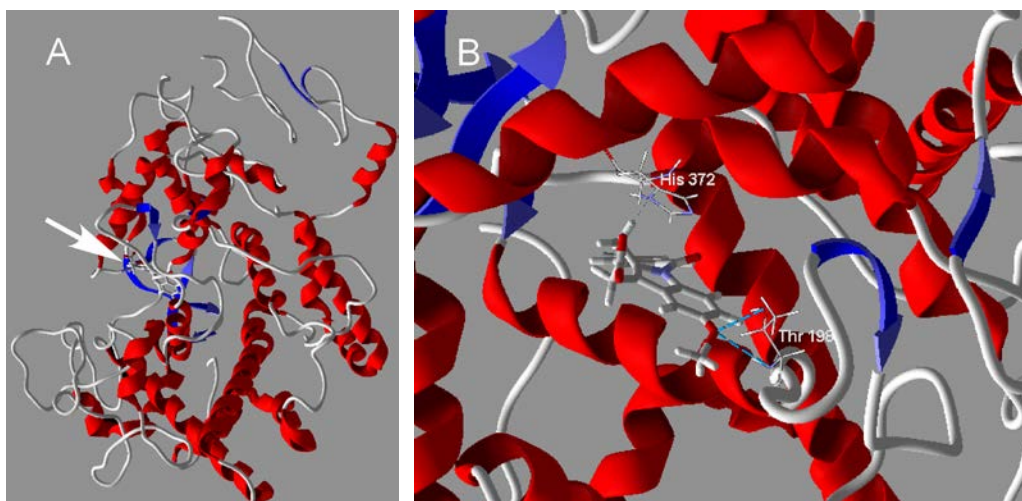
Figure 2-9. Interaction of indomethacin with COX2.
Indomethacin bound to COX2 pocket A (A). Methoxy group at indole skeleton (oxygen atom) of
indomethacin interacted with Thr[198], and carboxyl group (oxygen atom) interacted with His[372] (B).

Electrostatic potential interaction between TX-1123 and COX2.

The interactive feature of ESP fields between TX-1123 and COX2 was shown in Figure 2-10. An ESP field was not detected at the TX-1123-binding position, whereas positive (blue clouds) and negative (red clouds) ESP fields were distributed around the TX-1123-binding pocket (Figure 2-10). There were no ESP fields distribution at the celecoxib-binding position in COX2 molecule, but positive and negative fields were distributed around celecoxib-binding site.
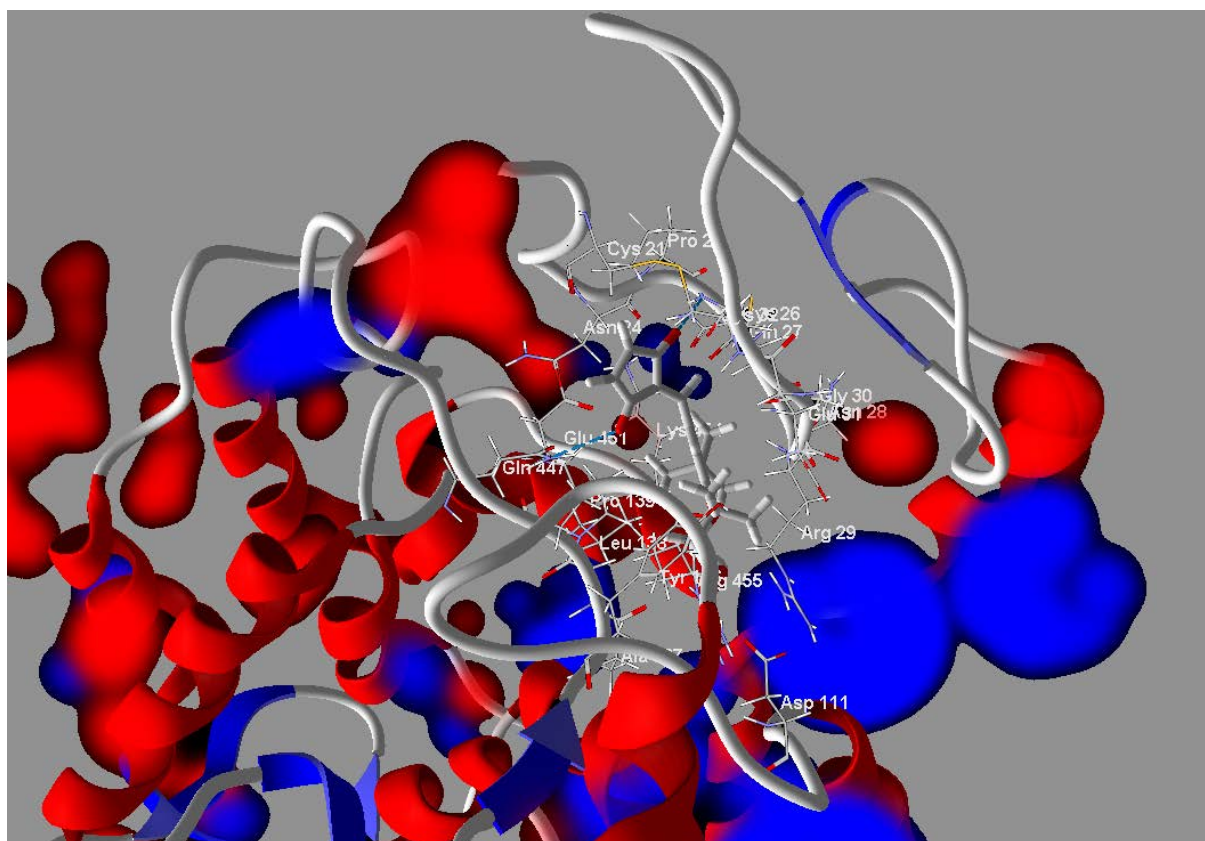
Figure 2-10.   ESP field profile of TX-1123-binding pocket of COX2.
Positive (blue clouds) and negative (red clouds) ESP fields were distributed around the TX-1123-binding pocket of COX2.

2-3-4. Discussion

The development of COX2-selective inhibitors were examined, and the molecular design and synthesis of TX-1123 derivatives were performed (Hori H. *et al.* (2002)). TX-1123 exhibited potent COX2-inhibitory activity, and the $R_{C1/C2}$ value of TX-1123 (13.5) was close to that of celecoxib (30.8) (Table 2-II). The $R_{C1/C2}$ value decreased to 4.63 for TX-1925, which possesses the methoxy group instead of the hydroxy group in TX-1123 (Figure 2-1). The $R_{C1/C2}$ value of TX-1918, which had two substituted methyl groups at the *tert*-butyl groups, decreased significantly to 0.11. The surrounding steric structure of the phenolic hydroxy group appears to be important for the COX2 selectivity. The $R_{C1/C2}$ value was 0.77 for TX-1926, which was introduced a benzene ring into the cyclopentene-1,3-dione region, and a conjugate system located far from the phenolic hydroxy group in TX-1123 may contribute to COX2 selectivity. It seemed to be not possible to confirm the COX2 selectivity of designed TX-1123 derivatives, except for TX-1123, which appears to be a useful lead steric structure for the design of more efficient compounds.

Three ligand-bindable pockets were observed in COX2 molecule (Figure 2-5), and the binding of TX-1123 to pocket B was detected by the binding simulation (Figure 2-6A). Celecoxib bound to pocket C of COX2, which differed from the TX-1123-bindable pocket (Figure 2-6C). The binding mechanism of TX-1123 to COX2 molecule was expected to differ from that of celecoxib. The IC_{50} value of TX-1123 was higher than the value of celecoxib, and the binding affinity of TX-1123 appeared to be weaker than that of celecoxib. TX-1123 was also bindable to COX1 molecule (pocket B), which differed from indomethacin-binding pocket (pocket C) (Figure 2-7C). The COX1-inhibitory activity of TX-1123 was one order weaker than that for COX2 (IC_{50} values in Table 2-II). COX1-inhibitory activity of indomethacin was two orders stronger than COX2-inhibitory activity, and the COX1-inhibitory mechanism of indomethacin appears to differ from the

inhibitory mechanism of TX-1123.

The ESP field did not exist at the TX-1123-bound COX2 pocket, and positive (blue clouds)-ESP and negative (red clouds)-ESP fields were surrounding the TX-1123-binding pocket (Figure 2-10). Thus, strong electrostatic energy does not appear to be necessary for the binding interaction between TX-1123 and COX2. A rigid interactive relationship, such as the lock-and-key model of enzyme and substrate, does not appear to be important for the COX2-selectivity of TX-1123 derivatives. Protein-ligand interactions have been examined using the isothermal titration calorimetry, and the molecular parameters (*e.g.* enthalpy, entropy) had been determined (Klebe G. (2015)). Enthalpy and entropy are used as components of the binding free energy, and these parameters are applied to molecular design. An optimized molecular which is highly efficient and has few side-effects exhibits more enthalpy dominated features (Freire E. (2008)). A dominant analysis of enthalpy with TX-1123 derivatives is currently in progress in order to obtain the better understanding of interaction mechanisms between TX-1123 derivatives and COX molecules.

Chapter 3. Molecular property of glyco-conjugated TX-1877 derivatives

3-1. Background

Sugars have a large number of hydroxyl groups, and can produce a wide variety of structures from combinations of bonding positions and bonding modes with sugars. In nature, sugars exist as free sugar chains, protein bound sugars, and lipid bound sugars. Sugar chains are not only linear polymers such as cellulose and chitin, but also branched molecules such as *N*-linked sugar chains and *O*-linked sugar chains, and various glyco-conjugated molecules are produced by the coordinated action of various glycosyltransferases (Chiba A. *et al.* (1997), Yoshida A. *et al.* (2001)). This "heterogeneity" controls the biochemical reaction of sugar chains. The role of sugar chains *in vivo* includes improving the molecular stability (*e.g.* water solubility, degradation resistance) and controlling the molecular interactions. The glycosylated peptides have increased blood retention, such as polyethylene glycol (PEG) modification. In antibody drugs, specific sugar chains have been reported to contribute to increased ADCC activity (Liu L. (2015)). In addition, sugar conjugated liposomes are used for drug delivery therapy.

A multifunctional molecular had been designed based on the structure of the hypoxic radiosensitizer 2-nitroimidazole acetamide (TX-1877). The designed molecules had radiosensitization, tumor growth-inhibition, metastasis-inhibition and immune system activation features (Kasai S. *et al.* (1998), Kasai S. *et al.* (2001), Abou-Bedair F.A. *et al.* (2002), Oshikawa T. *et al.* (2005)). Hori *et al.* investigated the effects of a bifunctional hypoxic cell radiosensitizer TX-1877 in augmenting anticancer host response. In syngeneic squamous cell carcinoma-bearing mouse model, single administration of TX-1877 significantly inhibited primary tumor growth as well as lung metastasis. TX-1877

administration resulted in a significant infiltration of immune cells (*e.g.* CD4^{+}T cell, CD8^{+}T cell, macrophage and dendritic cell (DC)), and increased the expression of chemokines for cytotoxic T lymphocyte (CTL), T helper 1 cell (Th1), monocyte macrophage and DC, in tumor tissues.   In tumor-draining lymph nodes, MHC class I-restricted CD8^{+} memory CTL specific for inoculated cancer cells were induced by TX-1877.   In experimental analysis, TX-1877 induced chemokines and inducible nitric oxide synthase (iNOS) in several types of cultured cells (Oshikawa T. *et al.* (2005)).

In order to explore the possibility of controlling molecular functions by adding sugar, sugar conjugated TX-1877 derivatives designed and the function control by sugar addition was verified.

3-2. Structure-associated functional control of TX-1877 derivatives by glyco-conjugation

3-2-1. Introduction

Sugar molecules have been effectively utilized in the drug design to improve water solubility and for molecular recognition. Tumor cells actively consume sugar, and the addition of a sugar moiety to the designed drugs improves their uptake by tumor tissues. Affinity of drugs to tumor cells may be enhanced by the conjugation of sugar structures. One of the strategies to potentially improve the affinity of designed compounds to tumor tissue is the sugar molecule conjugation to the pharmacophoric structure. Sugar-conjugated molecules designed to exploit this strategy had been examined (Pandey S.K. *et al.* (2007), Sylvaina I. *et al.* (2002)).

In the present report, structural features of the TX-1877 glyco-conjugated derivatives were examined. Designed and synthesized TX-1877 was more potent radiosensitizer than etanidazole, and exhibited additional biological activities, such as anti-metastatic and immunopotentiative activity (Kasai S. *et al.* (2001), Kasai S. *et al.* (1998), Abou-Bedair F.A. *et al.* (2002), Oshikawa T. *et al.* (2005)). TX-1877 was conjugated with several sugar molecules, such as β-glucose (β-Glc), β-galactose (β-Gal), α-mannose (α-Man), tetra-*O*-acetyl β-Glc (β-Glc(OAc)$_4$), tetra-*O*-acetyl β-Gal (β-Gal(OAc)$_4$), tetra-*O*-acetyl α-Man (α-Man(OAc)$_4$), *N*-acetyl-β-galactosamine (β-GalNAc), and tri-*O*-acetyl β-GalNAc (β-GalNAc(OAc)$_3$), and effects of the sugar molecules on structure-associated functional control of TX-1877 derivatives.

3-2-2. Materials and Methods

Molecular design and analysis.

TX-1877 and sugar conjugated TX-1877 derivatives were designed, and their molecular features were examined as previously described (Kasai S. *et al.* (1998), Oshikawa T. *et al.* (2005)). The conformation analysis of synthesized TX-1877 derivatives were performed using CAChe-Conflex (Fujitsu Inc., Tokyo, Japan), and the energy profiles were analyzed (Ohkura K. *et al.* (2005), Ohkura K. *et al.* (2003)). Solvation free energies (stereo-hydrophobicity: dGW) of TX-1877 derivatives were determined using Mopac (Fujitsu Inc., Tokyo, Japan) as previously described (Ohkura K. *et al.* (1999), Ohkura K. *et al.* (2007)).

In vitro radiosensitizing assay.

In vitro radiosensitization ability of synthesized TX-1877 derivatives were measured in EMT6/KU single cells under hypoxic conditions as previously described (Nakae T. *et al.* (2008), Shibamoto Y. *et al.* (1986)). Cells were suspended in test tubes (2.0×10^6 cells/mL MEM containing test compound) and tubes were made hypoxic by purging with gas mixture comprising 95% N_2-5% CO_2 for 60 min. Tubes were then irradiated using 6 MV X-rays generated by medical linear accelerator at dose rate of 2.0 Gy/min. After irradiation, cells were resuspended in MEM at appropriate concentrations and plated onto 6 cm culture dishes. After 5-7 days of culture, cells were plated in appropriate numbers to assay for colony-forming ability. Survival data were fitted with lines by the least-squares method. Enhancement ratio (ER) values were determined from the ratio of radiation doses required to reduce the surviving fraction of cells to 1%. Each ER value of radiosensitizer was obtained from the survival curves consisting of four or five points per curve and converted based on the ER value of etanidazole (ER=1.72) (Brown J.M. *et al.* (1980), Uto Y. *et al.* (2008)).

3-2-3. Results

Structure of glyco-conjugated TX-1877 derivatives.

Glyco-conjugated TX-1877 derivatives are shown in Figure 3-1. Monosaccharides were conjugated to the hydroxy group of TX-1877, and TX-1877 derivatives (β-glucose: TX-2141, β-galactose: TX-2218, and α-mannose: TX-2217) were synthesized. The hydroxyl groups of sugar moieties were acetylated, and the tetra-*O*-acetyl compounds (TX-2244, TX-2245, and TX-2246) were obtained. The *N*-acetyl group (-NHAc) or *N*-,*O*-acetyl group (-OAc, -NHAc) were added to the sugar moiety of TX-2218, and TX-2068 (*N*-acetylated) or TX-2243 (*N*-, *O*-acetylated) were obtained (Nakae T. *et al.* (2008)).
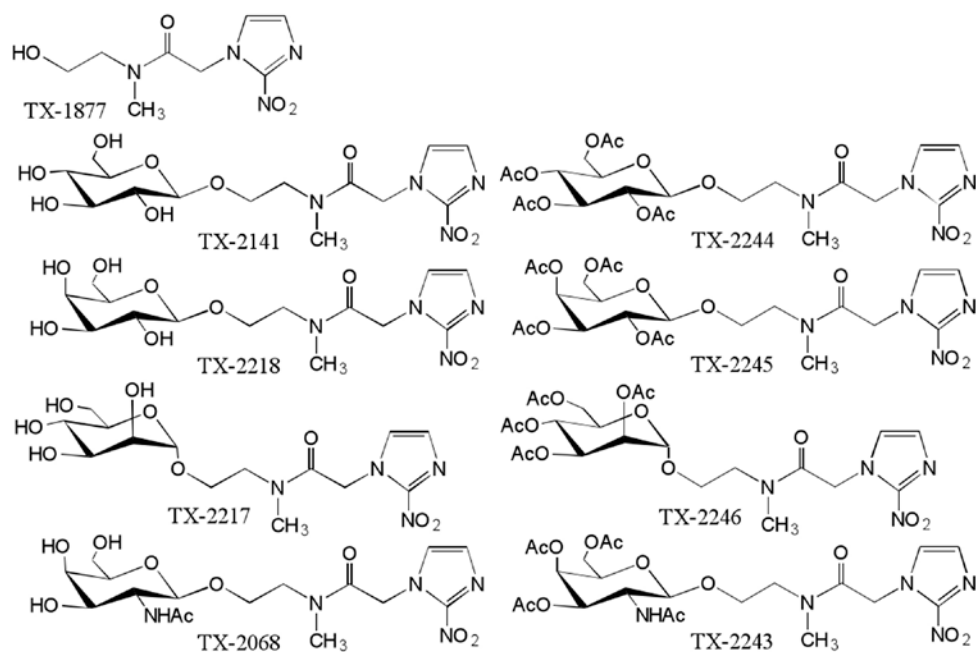
Figure 3-1.   Structure of sugar-conjugated TX-1877 derivatives.

Table 3-I. Conformer and enhancement ratios (ER) of TX-1877 derivatives.

Compound	Conformer No.	Energy (kcal/mol)[a]	dGW (kJ/mol)[b]	ER[c]
TX-1877	71	16.245	-157.664	1.75
TX-2141	402	34.318	-196.704	1.33
TX-2218	333	33.216	-200.945	1.40
TX-2217	357	33.838	-206.721	1.41
TX-2244	517	12.592	-248.576	2.30
TX-2245	659	13.551	-259.976	1.63
TX-2246	548	12.490	-247.198	1.88
TX-2068	235	20.257	-205.766	1.43
TX-2243	334	4.708	-255.787	1.47

[a]Average of heat formation energy (kcal/mol).
[b]Average of solvation free energy (kJ/mol).
[c]Nakae T. *et al.* (2008).

Energy profiles of glyco-conjugated derivatives.

TX-1877 generated 71 conformers during conformation analysis (Table 3-I).   Their heat formation energies ranged between 12.881 and 18.520 kcal/mol (Figure 3-2A), and the average was 16.245 kcal/mol (Table 3-I).   The average of solvation-free energy (dGW: an index of stereo-hydrophobicity, lower dGW value means higher hydrophobicity) of TX-1877 was -157.664 kJ/mol (Figure 3-2E).   The β-glucose-conjugated TX-2141 had 402 conformers (27.712 − 43.694 kcal/mol, average: 34.318 kcal/mol), and their dGW values decreased from -169.989 kJ/mol to -238.085 kJ/mol (average: -196.704 kJ/mol) (Figure 3-2B and 3-2F).   TX-2218 and TX-2217 had 333 (24.177 − 45.751 kcal/mol, average: 33.216 kcal/mol) and 357 (26.307 − 42.406 kcal/mol, average: 33.838 kcal/mol) conformers, respectively (Figure 3-2C and 3-2D).   The dGW values of TX-2218 (-245.781 − -165.799 kJ/mol, average: -200.945 kJ/mol, Figure 3-2G) and TX-2217 (-223.697 − -187.758 kJ/mol, average: -206.721 kJ/mol, Figure 3-2H) decreased during the conformational analysis.   The molecular hydrophobicities of sugar-conjugated TX-1877 derivatives increased with increments of their heat formation energies.
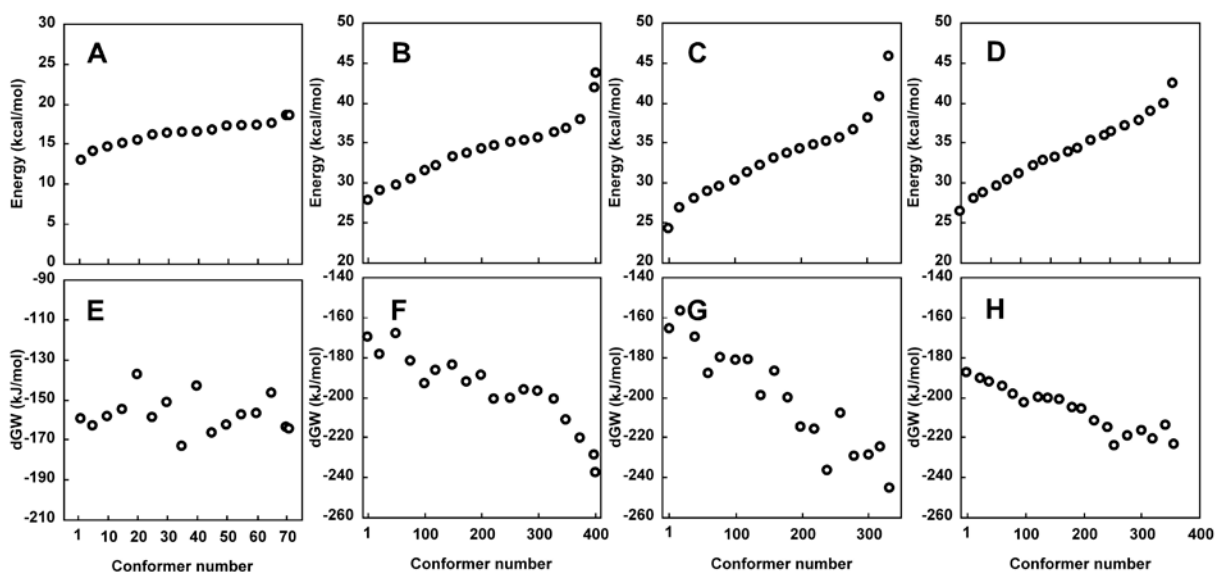
Figure 3-2.   Energy profile of conformation analysis of monosaccharide conjugated TX-1877 derivatives.
Profiles between conformer and heat formation energy of TX-1877 (A), TX-2141 (B), TX-2218 (C), TX-2217 (D).   Profiles between conformer and solvation free energy (dGW) of TX-1877 (E), TX-2141 (F), TX-2218 (G), TX-2217 (H).

More conformers were detected in the conformational analysis of tetra-O-acetyl-modified TX-1877 derivatives (TX-2244, TX-2245, and TX-2246) than in that of monosaccharide conjugated derivatives (*e.g.* TX-2141, TX-2218, and TX-2217). TX-2244 had 517 conformers (7.616 − 21.798 kcal/mol, average: 12.592 kcal/mol, Figure 3-3A), and dGW values decreased from -229.050 to -282.717 kJ/mol (average: -248.576 kJ/mol) (Figure 3-3D).   TX-2245 and TX-2246 had 659 (7.521 − 28.315 kcal/mol, average: 13.551 kcal/mol, Figure 3-3B) and 548 (6.082 − 20.343 kcal/mol, average: 12.490 kcal/mol, Figure 3-3C) conformers, respectively.   Their dGW values decreased during the conformational analysis (TX-2245: from -245.247 to -280.686 kJ/mol (average: -259.976 kJ/mol) (Figure 3-3E), TX-2246: from -228.881 to -264.405 kJ/mol (average: -247.198 kJ/mol) (Figure 3-3F)).   Heat formation energies decreased with the tetra-O-acetylation of sugar moieties, and molecular stability increased.   The dGW values of O-acetylated TXs (*e.g.*, TX-2244, TX-2245, and TX-2246) decreased than those of monosaccharide conjugated TX-1877 derivatives, and their hydrophobicities were increased by O-acetylation.

33
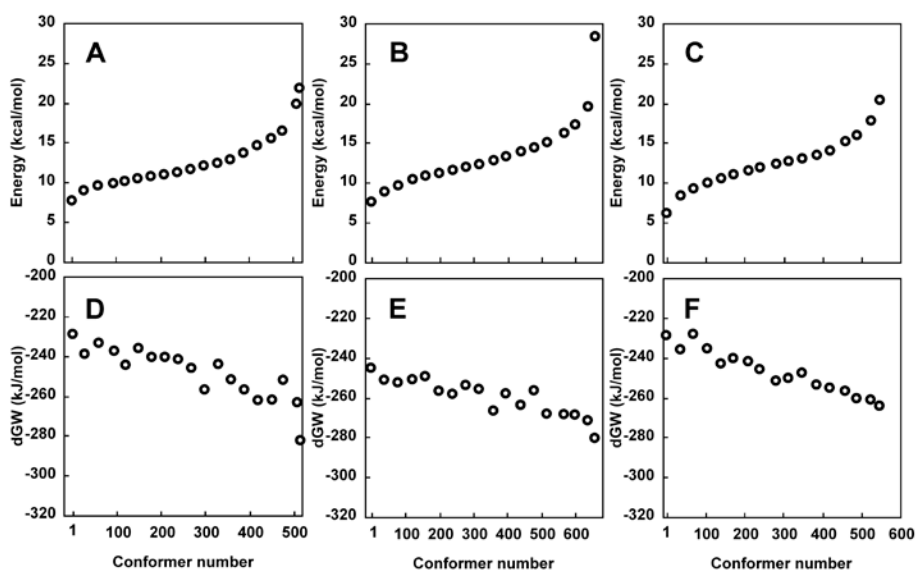
Figure 3-3.   Energy profile and stereo-hydrophobicity of tetra-*O*-acetylated TX derivatives.
Profiles between conformer and heat formation energy of TX-2244 (A), TX-2245 (B), TX-2246 (C).
Profiles between conformer and solvation free energy of TX-2244 (D), TX-2245 (E), TX-2246 (F).

The *N*-acetylation of TX-2218 caused an increase in molecular stability, and heat formation energy decreased from 24.177 kcal/mol (Figure 3-2C, global minimum (GM) conformer of TX-2218) to 10.353 kcal/mol (Figure 3-4A, the GM conformer of TX-2068). The *N*-, *O*-acetylation of TX-2218 significantly increased molecular stability, and heat formation energy decreased (-4.344 kcal/mol in Figure 3-4B, the GM conformer of TX-2243).

The relationship between conformers and hydrophobicity was unaffected by the *N*-acetylation of TX-2218, and the dGW profile of TX-2068 (Figure 3-4C, -225.846 − -185.364 kJ/mol, average: -205.766 kJ/mol) was similar to that of TX-2218. Stereo-hydrophobicity was increased by the *N*-, *O*-acetylation of TX-2218, and a lower dGW value was obtained in the TX-2243 analysis (Figure 3-4D, -271.989 − -240.330 kJ/mol, average: -255.787 kJ/mol).
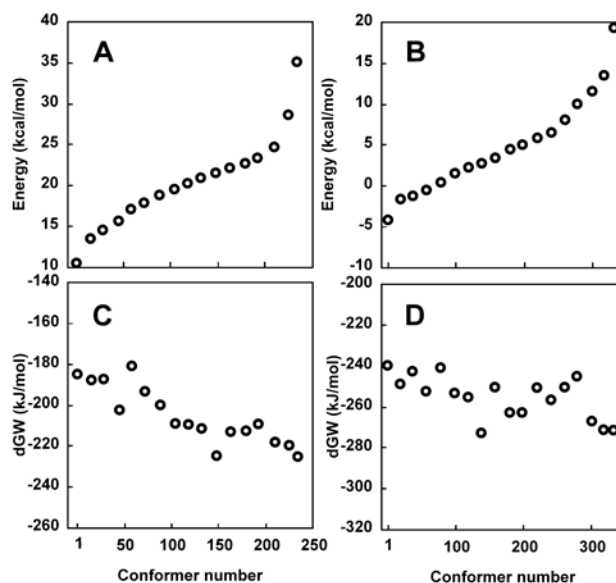
Figure 3-4.   Molecular features of *N*-acetylated and *N*-, *O*-acetylated derivatives.
Profiles between conformer and energy of TX-2068 (A), TX-2243 (B).
Profiles between conformer and dGW of TX-2068 (C),TX-2243 (D).

Radiosensitizing activity of TX-1877 derivatives.

The radiosensitizing activities of sugar-conjugated TX-1877 derivatives were examined *in vitro* at a dose of 1 mM in EMT6/KU cells under the hypoxic conditions.   The ERs were shown in Table 3-I, and the ER of TX-1877 was 1.75.   ER values of non-acetylated sugar conjugated TX-1877 derivatives (TX-2141: ER=1.33, TX-2218: ER=1.40, TX-2217: ER=1.41) were lower than that of etanidazole (ER=1.72) (Brown J.M. *et al.* (1980)), and they did not exhibit any radiosensitizing activity.   Thus their radiosensitizing activities were suppressed by sugar conjugation.   In the tetra-*O*-acetylated compounds, TX-2244 and TX-2246 exhibited radiosensitizing activities, with that of TX-2244 being significant (ER=2.30).   *N*-acetylated   TX-2068 (ER=1.43) and *N*-,*O*-acetylated TX-2243 (ER=1.47) showed an ER decrease from TX-1877 (ER=1.75).

35

3-2-4. Discussion

The designed derivatives were synthesized with a conjugated sugar molecule in anticipation of their precipitative incorporation into cancer cells (Pandey S.K. *et al.* (2007), Sylvaina I. *et al.* (2002), Mikata Y. *et al.* (2001), Idutsu Y. *et al.* (2005), Toshima K. *et al.* (2004), Toshima K. *et al.* (2003), Toshima K. *et al.* (2002)).   The heat formation energy (*i.e.* an index of molecular destabilization) of monosaccharide-conjugated TX-1877 derivatives (TX-2141, TX-2218, TX-2217) were greater than that of the parent TX-1877 molecule.   This result indicated that the reactivity of the monosaccharide-conjugated compounds were greater than that of TX-1877.   Moreover, the heat formation energies of tetra-*O*-acetylated compounds   (TX-2244,   TX-2245,   TX-2246)   were   lower   than   those   of monosaccharide-conjugated compounds (TX-2141, TX-2218, TX-2217), and these molecules were stabilized by *O*-acetylation.   In the conformation analysis of TX-1877, a correlation was not observed between the stability and the hydrophobicity, and its dGW average value was -157.664 kJ/mol.   In monosaccharide- or tetra-*O*-acetyl-conjugated TX compounds, the stereo-hydrophobicity (dGW) increased with a decrease in the stability (heat formation energy) (Figure 3-2, Figure 3-3).   The conformations and the hydrophobicities of designed compounds   seem   to   be   controlled   by   the   addition   of   a   monosaccharide-   or tetra-*O*-acetyl-conjugated sugar to TX-1877.   The tetra-*O*-acetylation of β-glucose moiety of parent TX-2141 molecule significantly improved the radiosensitizing efficacy (TX-2244). Acetylation of hydroxyl group in the glucose moiety appears to be advantageous for the radiosensitization.   Regarding TX-2244, the balance between the molecular stability and the hydrophobicity was thought to work advantageously for the radiosensitization ability.

ER was not increased by the *N*-acetylation of the β-galactose moiety (TX-2068).   A strong ER-potentiating effect was not observed with the *N*-, *O*-acetylation of galactose (TX-2243).   Based on these results, it can be speculated that the modification of glucose in

the TX molecular design improves ER.   Radiosensitization is now being investigated for TX-1877 derivatives with a conjugated disaccharide or polysaccharide moiety.

The hydrophobicities of tetra-*O*-acetylated compounds (*e.g.* TX-2244, TX-2245, and TX-2246) were high, and the dGW values were -259.976 − -247.198 kJ/mol (Table 3-I). The hydrophobicities of monosaccharide-conjugated compounds (TX-2141, TX-2218, TX-2217: Figure 3-2F, 3-2G, 3-2H) were not higher than those of tetra-*O*-acetylated compound (TX-2244, TX-2245, TX-2246: Figure 3-3D, 3-3E, 3-3F).   The interaction between *in vivo* water molecules and TX-1877 derivatives appear to control radiosensitizing activity (*e.g.* ER) through stereo-hydrophobicity.   In the electrostatic potential (ESP) field analysis of TX-1877 and TX-2244, positive and negative ESP field developed with entire molecule evenly (Figure 3-5 and Figure 3-6).   A detailed analysis of ESP field participation in radiosensitizing activity is in progress.
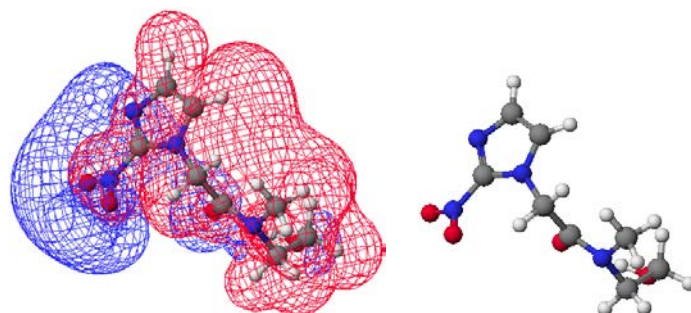
Figure 3-5.   ESP distribution of TX-1877.
Left panel: Positive (red mesh) and negative (blue mesh) fields distributed.   Right Panel: TX-1877 molecule.
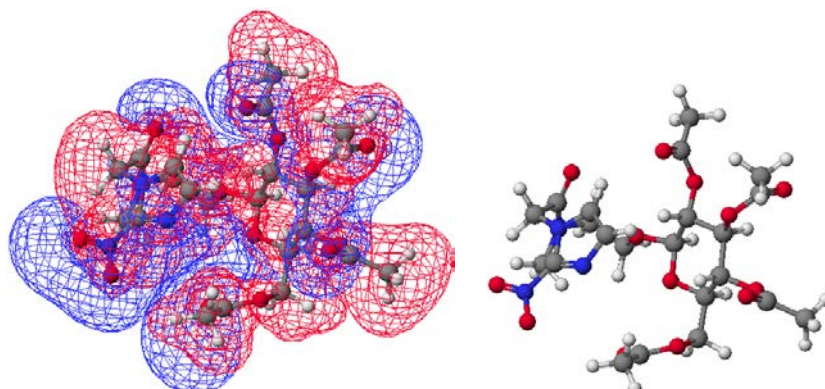
Figure 3-6.   ESP distribution of TX-2244.
Left panel: Positive (red mesh) and negative (blue mesh) fields distributed.   Right panel: TX-2244 molecule.

Chapter 4.　Molecular chirality and interactive ability of TX-2036 derivatives

4-1.　Background

The chiral 2-nitroimidazole derivatives containing a 2-aminomethylene-4-cyclopentene-1,3-dione moiety had been designed as antiangiogenic hypoxic cell radiosensitizers (Figure 4-1) (Nagasawa H. *et al.* (2006)). The 2-aminomethylene-4-cyclopentene-1,3-dione moiety was expected to show high electrophilicity than the 2-methylene-4-cyclopentene-1,3-dione moiety by molecular orbital calculations. TX-2036 is including the 2-aminomethylene-4-cyclopentene-1,3-dione structure, and proved to be the strong antiangiogenic hypoxic cell radiosensitizer (Uto Y. *et al.* (2008)). TX-2036 derivatives have been synthesized, and their ability as the antiangiogenic hypoxic cell radiosensitizer have been examined.
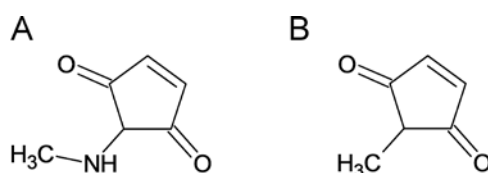
Figure 4-1.　Structure of 4-cyclopentene-1,3-dione
A: 2-aminomethylene-4-cyclopentene-1,3-dione.
B: 2-methylene-4-cyclopentene-1,3-dione

TX-2036 has a chiral center (Figure 4-2), and generated a stereoisomer. Structures with different sizes (*e.g.* methyl, *tert*-butyl, *p-tert*-butyl) was added to the chiral center, and their radiosensitizing ability was verified. In addition, the radiosensitizing ability of each enantiomeric pair was compared, and the three-dimensional structural factors that affect the

sensitizing ability were examined. As comparing the structural features, molecular parameters such as heat formation energy (an index for reactivity), solvation free energy (dGW: index for stereo-hydrophobicity), electrostatic potential (ESP: index for interaction) were used.

The protein kinase (PTK) inhibitory activity of TX-2036 was examined, and it showed potent EGF-receptor (EGFR) kinase inhibition, having an IC_{50} value was lower than 2 μM (Uto Y. *et al.* (2008)). TX-2036 also showed Flt-1 kinase inhibition, having an IC_{50} value was lower than 20 μM. The chiral TX-2036 molecule contains the 2-aminomethylene-4-cyclopentene-1,3-dione structure as a potent pharmacophoric descriptor is promising lead candidates for the development of biological active compounds (*e.g.* antiangiogenic hypoxic cell radiosensitizers, PTK inhibitors). In this chapter, the EGFR kinase inhibitory ability of TX-2036 derivatives were examined, and the interactive features between TX-2036 derivatives and EGFR kinase domain were discussed.

4-2. Correlation between radiosensitizing ability and stereo-structure of the TX-2036 series of molecules

4-2-1. Introduction

Design, synthesis, and evaluation of racemic and enantiomerically pure chiral haloacetylcarbamoyl-2-nitroimidazoles, including chloro- and bromo-derivatives, as antiangiogenic hypoxic cell radiosensitizers were performed (Jin C.Z. *et al.* (2004)).   In the tumor microenvironment, there are the soft nucleophiles such as nonprotein thiol and thiol protease.   Therefore, the strategy was developed to design 2-nitroimidazole derivatives that incorporate a soft electrophile, the aminomethylene-cyclopentenedione moiety, as the new anti-angiogenic and anti-tumor functional group.

Two potential benefits of the chiral center for designed hypoxic cell radiosensitizers were considered.   First, this would provide us with two molecular structures that have different biological activities from the same synthetic route.   Second, each enantiomer would possess specific pharmacokinetic and pharmacodynamic properties.   The 2-nitroimidazole based TX-2036 series, which had the 2-aminomethylene-4-cyclopentene-1,3-dione structure as the anti-angiogenic pharmacophoric descriptor, were designed, synthesized, and evaluated their features (Uto Y. *et al.* (2008)).

4-2-2. Materials and Methods

Energy analysis of the TX-2036 derivatives.

The TX-2036 and its derivatives were designed and synthesized as previously described (Uto Y. *et al.* (2008)).   Conformation analysis of synthesized TX-2036 derivatives were performed using CAChe-Conflex (Fujitsu Inc., Tokyo, Japan), and their energy profiles were obtained as previously described (Ohkura K. *et al.* (2003), Ohkura K. *et al.* (2005)). Solvation free energies (stereo-hydrophobicity: dGW) of TX-2036 derivatives were determined using Mopac (Fujitsu Inc.) as previously described (Ohkura K. *et al.* (1999), Zhu, J.W. *et al.* (2000)).   Electrostatic potential (ESP) fields of designed TX-2036 derivatives were analyzed using CAChe (Fujitsu Inc.) as previously described (Ohkura K. *et al.* (2009)). The ESP field analysis was performed for the minimum energy conformer (*i.e.* global minimum conformer) of each TX-2036 derivative.

In vitro radiosensitizing assay.

In vitro radiosensitization of designed compounds were measured in EMT6/KU single cells under hypoxic conditions as previously described (Nakae T. *et al.* (2008), Shibamoto Y. *et al.* (1986)).   The enhancement ratios (ERs) were determined from the ratio of radiation doses required to reduce the surviving fraction of EMT6/KU cells to 1%.   Each ER value of radiosensitizer was obtained from survival curves consisting of four or five points per curve and converted based on the ER value of etanidazole (ER=1.72, Figure 4-2C) (Uto Y. *et al.* (2008), (Brown J.M. *et al.* (1980)).

4-2-3.   Results

Molecular profiles of TX-2036 derivatives.

Structures of designed TX-2036 derivatives are shown in Figure 4-2.   These compounds had a chiral center and were classified into *R*-configurations (TX-2043, TX-2030, TX-2036) or *S*-configuration (TX-2044, TX-2031, TX-2037).   The radiosensitizing activity of *R*-configured TX-2043 (ER=1.80) was weaker than that of *S*-configured TX-2044 (ER=2.00) (Table 4-I).   In other TX-pairs, the radiosensitizing activity of *R*-configured TXs was weaker than that of *S*-configured TXs (TX-2030 (ER=1.68) vs. TX-2031 (ER=1.80), TX-2036 (ER=1.79) vs. TX-2037 (ER=1.93)).   Moreover, the radiosensitizing activity of *R*-configured TX-2045 (ER=2.02) having 2,2,2,-trifluoroacetylamino group was stronger than that of *S*-configured TX-2046 (ER=1.84).
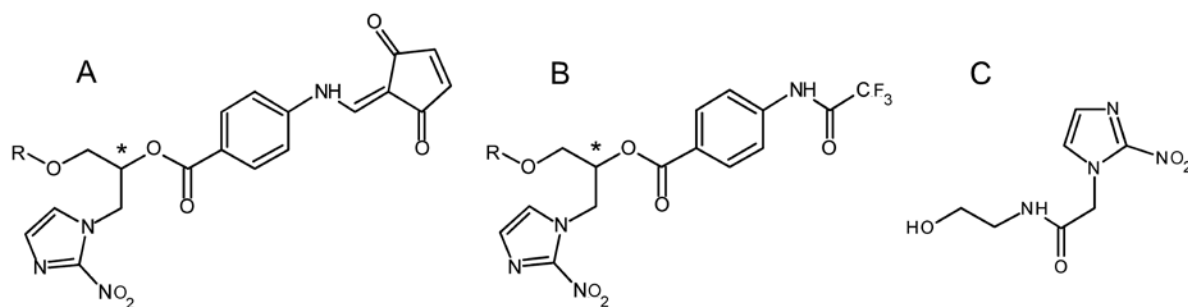
Figure 4-2.   Structure of TX-2036 derivatives.
TX-2036 derivatives have chiral center (*), and formed enantiomer pairs.
(A)   TX-2043: *R*-configuration, R=methyl, TX-2044: *S*-configuration, R=methyl,
       TX-2030: *R*-configuration, R=*tert*-butyl, TX-2031: *S*-configuration, R=*tert*-butyl,
       TX-2036: *R*-configuration, R=*p-tert*-butyl, TX-2037: *S*-configuration, R=*p-tert*-butyl
(B)   TX-2045: *R*-configuration, R=methyl, TX-2046: *S*-configuration, R=methyl
(C)   Etanidazole

Table 4-I.   Radiosensitizing activity of TX-2036 derivatives

Compounds	ER (concentration)
Etanidazole	1.72 (1 mM)
TX-2043	1.80 (1 μM)
TX-2044	2.00 (1 μM)
TX-2030	1.68 (1 μM)
TX-2031	1.80 (1 μM)
TX-2036	1.79 (1 μM)
TX-2037	1.93 (1 μM)
TX-2045	2.02 (1 μM)
TX-2046	1.84 (1 μM)

ER (concentration): enhancement ratio at corresponding concentration.

The energy profiles of enantiomer pairs (*e.g.* TX-2030 and TX-2031 pair (13.8 − 27.0 kcal/mol), TX-2036 and TX-2037 pair (4.7 − 18.6 kcal/mol), TX-2043 and TX-2044 pair (8.8 − 22.9 kcal/mol), TX-2045 and TX-2046 pair (60.7 − 67.3 kcal/mol)) were almost unchanged by their stereo-configuration during conformation analysis (open circles in Figure 4-3).   The solvation free energy (an index of the stereo-hydrophobicity) profiles of these enantiomer pairs did not differ (*e.g.* TX-2030 and TX-2031 pair (-218.9 − -194.4 kJ/mol), TX-2036 and TX-2037 pair (-229.1 − -195.1 kJ/mol), TX-2043 and TX-2044 pair (-232.6 − -204.5 kJ/mol), TX-2045 and TX-2046 pair (-208.7 − -178.5 kJ/mol)) (closed circles in Figure 4-3).
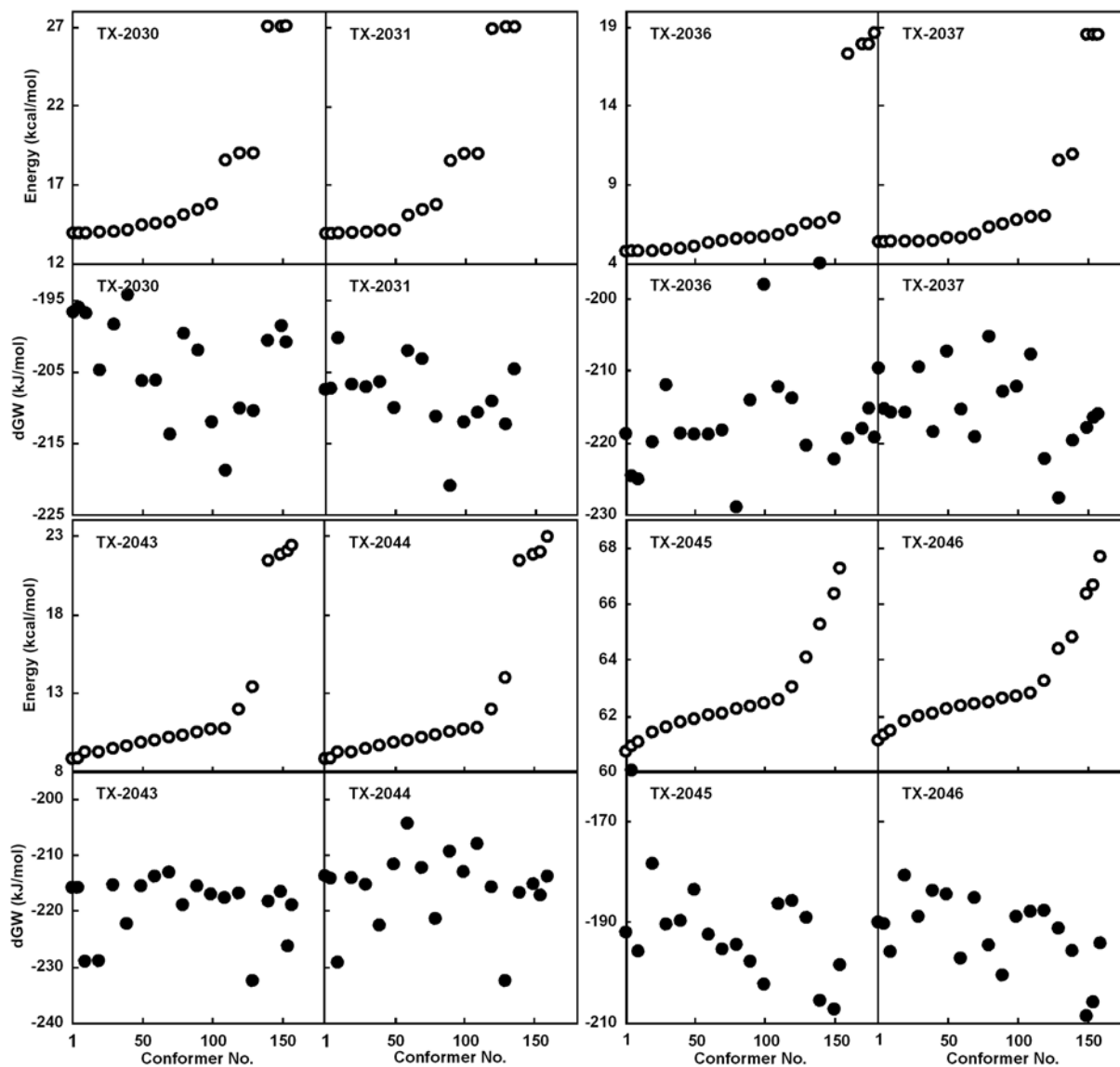
Figure 4-3.   Energy profiles of conformation analysis of TX-2036 derivatives.
Conformer-energy profiles of TX-2030, TX-2031, TX-2036, TX-2037, TX-2043, TX-2044, TX-2045, TX-2046 are shown in upper panels (open circles). Conformer-solvation free energy (dGW) profiles of TX-2030, TX-2031, TX-2036, TX-2037, TX-2043, TX-2044, TX-2045, TX-2046 are shown in lower panels (closed circles).

Electrostatic potential fields of TX-2036 derivatives.

The electrostatic potential (ESP) fields of the TX-2030 and TX-2031 enantiomer pair were similar, but small minus ESP field was observed in the cyclopentene-1,3-dione portion of *R*-configured TX-2030 (arrowheads in Figure 4-4). ESP fields of the TX-2036 and TX-2037 pair were similar each other, but small minus ESP field was observed in the cyclopentene-1,3-dione region of *R*-configured TX-2036 as well as TX-2030 molecule

44

(arrowheads in Figure 4-4).   In the TX-2043 and TX-2044 pair, the ESP fields were similar,

but two small minus ESP fields were observed in the cyclopentene-1,3-dione portion of

R-configured TX-2043 (arrowheads).   In the TX-2045 and TX-2046 pair, ESP fields were

similar, but two small minus fields were observed in the 2,2,2-trifluoroacetylamino group

(arrowheads) of *S*-configured TX-2046.   TX-2036 derivatives with these small minus fields

indicated weaker radiosensitizing activity than in the corresponding stereoisomers (Table 4-I).
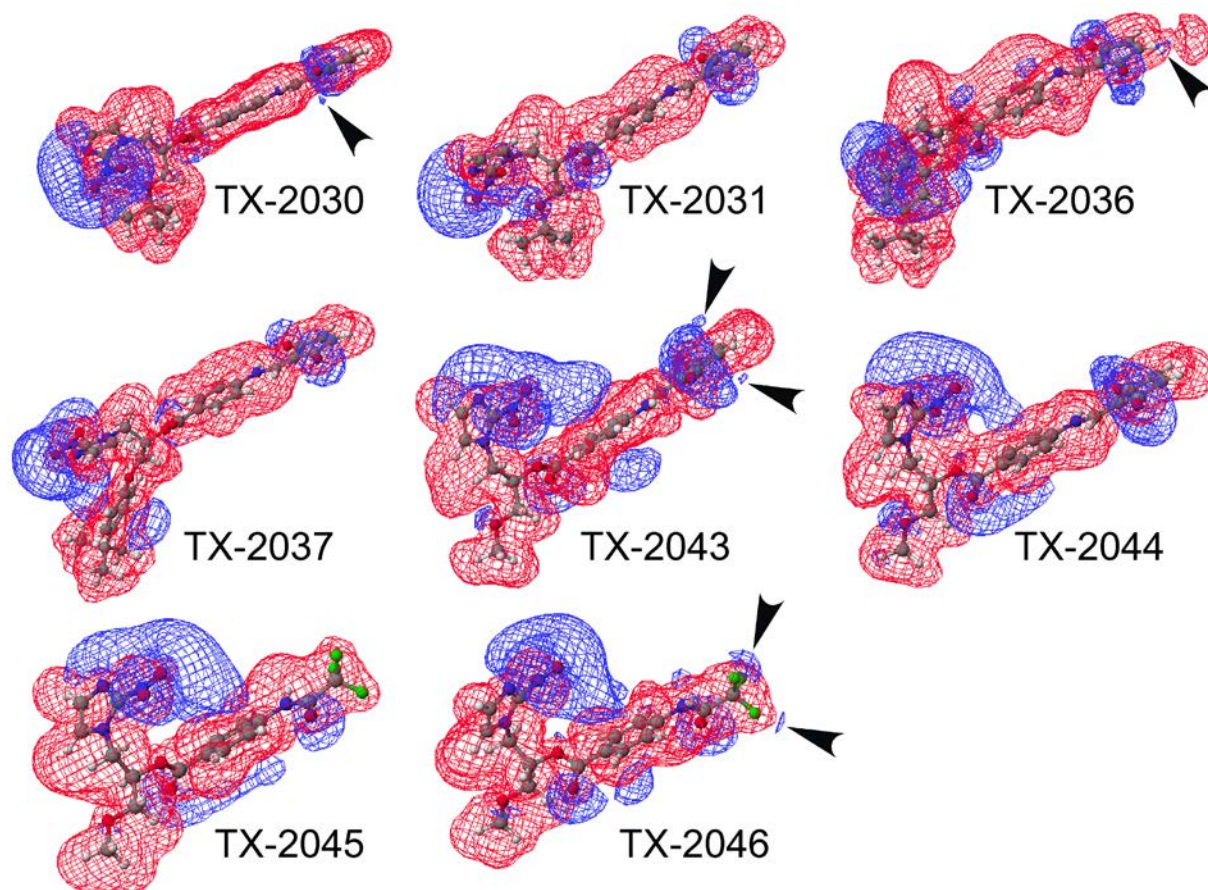
Figure 4-4.   Electrostatic potential (ESP) field of TX-2036 derivatives.
Positive and negative fields are shown as red and blue clouds, respectively.
Small minus ESP fields are shown as arrowheads.

4-2-4.　Discussion

Synthesized TX-2036 *S*-derivatives (TX-2044, TX-2031, and TX-2037) had stronger radiosensitizing activity than the corresponding *R*-derivatives (TX-2043, TX-2030, and TX-2036) (Table 4-I).　Conformation profile and stereo-hydrophobicity analysis did not reveal a difference between the *S*- and *R*-configured TX-2036 derivatives (Figure 4-3).　In the electrostatic potential field analysis, small minus ESP fields were observed only in *R*-configurations (TX-2043, TX-2030, and TX-2036) in the cyclopentene-1,3-dione region (Figure 4-4).　These small minus fields influenced the radiosensitizing activity.　The radiosensitizing activity of TX-2046 (*S*-configuration) with small ESP field was lower than that of TX-2045 (*R*-configuration), which suggests that the small ESP fields affect their radiosensitizing activity.　The ESP field is a barrier that develops on the surface of the structure generating it.　The positive and negative fields do not attract materials with same charge (*e.g.* ligand, solvent).　Even the smallest ESP field seems to affect the interaction between materials.

The TX-2036 derivatives have two characteristic structures, such as the 2-nitroimidazole site and the 4-cyclopentene-1,3-dione site.　The 2-nitroimidazole structure involved TX-1877 derivatives were developed and examined the correlation between structure and radiosensitizing activity (Ohkura K. *et al.* (2019), Miyake K. *et al.* (2008)).　In the TX-2036 derivatives, the 4-cyclopentene-1,3-dione structure may play a role in functional modification via small ESP field distribution.　For this reason, effective radiosensitizing activity seems to be obtained by modification of the 4-cyclopentene-1,3-dione structure.

4-3. Effect of isomerization of TX-2036 derivatives on interaction with tyrosine kinase domain of EGF receptor

4-3-1. Introduction

The molecular design and evaluation of enantiomerically pure chiral haloacetylcarbamoyl-2-nitroimidazoles (TX-1898 derivatives), including chloro- and bromo-derivatives, as antiangiogenic hypoxic cell radiosensitizers had been examined (Jin C.Z. *et al.* (2004)). In the tumor microenvironment, softer nucleophiles such as non-protein thiols and thiol proteases exist. The 2-nitroimidazole derivatives that incorporate a softer electrophile, the aminomethylenecyclopentenedione moiety, as the antiangiogenic and antitumor functional group were designed. Effect of the molecular chirality and the side chain bulkiness of designed 2-nitroimidazole derivatives on biological activities had been examined (Ohkura K. *et al.* (2007)). Two potential benefits of having a chiral center in the hypoxic cell radiosensitizers were considered. First, enantiomers provide two molecular structures expected to exhibit different biological activities from the same synthetic route. Second, each enantiomer exhibits a specific pharmacokinetic, pharmacodynamic property. Moreover, 2-nitroimidazole-based antiangiogenic hypoxic cell radiosensitizers (TX-2036 derivatives) that incorporate the 2-aminomethylene-4-cyclopentene-1,3-dione structure was designed (Uto Y. *et al.* (2008)). Radiation sensitizing ability of TX-2036 derivatives were influenced by structure of chiral-2-nitroimidazole region (Ohkura K. *et al.* (2019)). TX-2036 derivatives exhibited a protein kinase (*e.g.* EGF receptor involved tyrosine kinase domain) inhibition, and the *R*-configured derivatives showed more potent inhibitory activity than *S*-configured derivatives. In the present chapter, interactive analyses were performed between TX-2036 derivatives and tyrosine kinase domain of EGFR (EGFR-tyk) .

4-3-2. Materials and Methods

Assay for EGFR involved tyrosine kinase activity.

A431 human epithelial carcinoma cells were solubilized and cell debris was removed. Cell lysate was incubated with or without EGF at 25 $^{\circ}$C for 30 min, and the reaction was started by addition of $[\gamma\text{-}^{32}P]$ATP and incubated at 0 $^{\circ}$C for 10 min.   After the reaction was stopped, the mixture was washed.   Phosphorylation of the EGF receptor was estimated as the ^{32}P radioactivity using a scintillation counter (Uto Y. *et al.* (2008), Murakami Y. *et al.* (1994)).

Interactive analysis between TX-2036 derivatives and EGFR-tyk.

X-ray data of the protein kinase domain of EGFR was obtained from Protein Data Bank (ID = 1M17).   TX-2036 derivatives were synthesized as previously described (Uto Y. *et al.* (2008)), and conformation analyses were performed using CAChe-Conflex (Fujitsu Inc., Tokyo, Japan) (Ohkura K. *et al.* (2003), Ohkura K. *et al.* (2005)).   Interactive analysis of TX-2036 derivatives with protein kinase domain of EGFR was performed using Molegro Virtual Docker (CLC bio., Aarhus, Denmark) as preciously described (Ohkura K. *et al.* (2016), Ohkura K. *et al.* (2017)).   The ligand-bindable pockets of protein kinase domain of EGFR were examined using Molegro Virtual Docker.
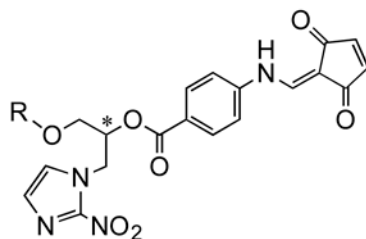
Figure 4-5.   Structure of TX-2036 derivatives.
*R-configuration: TX-2043 (R=methyl), TX-2030 (R=*tert*-butyl), TX-2036 (R=*p-tert*-butyl).
*S-configuration: TX-2044 (R=methyl), TX-2031 (R=*tert*-butyl), TX-2037 (R=*p-tert*-butyl).

4-3-3. Results

Tyrosine kinase inhibitory activities of TX-2036 derivatives.

Structures of TX-2036 derivatives were shown in Figure 4-5. These compounds had chiral center, and they were classified into *R*-configuration (TX-2043, TX-2030, and TX-2036) and *S*-configuration (TX-2044, TX-2031, and TX-2037). In methyl group containing derivatives, *R*-configured TX-2043 inhibited the EGFR-tyk activity and the IC_{50} was 2.3 µM (Table 4-II). EGFR-tyk inhibition of *S*-configured TX-2044 was weaker than that of TX-2043, and the IC_{50} value was 23.0 µM. TX-2030 (*tert*-butyl containing *R*-configured) more strongly inhibited EGFR-tyk (IC_{50} = 21.3 µM) than TX-2031 (*tert*-butyl containing *S*-configured) (IC_{50} = 213.0 µM). EGFR-tyk inhibition of *p-tert*-butyl containing TX-2036 (*R*-configured, IC_{50} = 1.8 µM) was stronger than that of TX-2037 (*S*-configured, IC_{50} = 18.4 µM).

Table 4-II.   Effect of TX-2036 derivatives on tyrosine kinase activities.

TXs (chirality)	IC_{50} (µM)[a]
TX-2043 (*R*)	2.3
TX-2044 (*S*)	23.0
TX-2030 (*R*)	21.3
TX-2031 (*S*)	213.0
TX-2036 (*R*)	1.8
TX-2037 (*S*)	18.4

[a]Uto Y. *et al.* (2008).

Interaction between TX-2036 derivatives and tyrosine kinase domain of EGFR.

Tyrosine kinase domain of EGFR (PDB ID = 1M17) had ligand-bindable sites (green clouds in Figure 4-6). TX-2043 became trapped in ligand bindable site of EGFR-tyk, and interacted with EGFR-tyk Lys[721] (main chain amino group) and Thr[766] (side chain hydroxyl

group) by 2-nitroimidazole region (Figure 4-7, Figure 4-8, Table 4-III, and Figure 4-9). TX-2044 interacted with EGFR-tyk Ile[765] (main chain amino group) and Thr[766] (side chain hydroxyl group) by 2-nitroimidazole. The *tert*-butyl containing TX-2030 interacted with Lys[721] (main chain amino group) and Thr[766] (side chain hydroxyl group) by 2-nitroimidazole. Target amino acid residues of TX-2031 differed from those of TX-2030, and TX-2031 interacted with Ser[696] (main chain amino group) by 1,3-cyclopentene dione region, Thr[766] (side chain hydroxyl group) and Thr[830] (side chain hydroxyl group) by 2-nitroimidazole region. TX-2036 interacted with Lys[721] (main chain amino group) by 1,3-cyclopentene dione and Thr[766] (side chain hydroxyl group) by nitrogen atom near 1,3-cyclopentene dione. TX-2037 interacted with different amino acid residues from TX-2036, and acted on Gly[772] (amino group) by oxygen atom near benzene ring, Cys[773] (thiol and amino group) by 2-nitroimidazole and Thr[830] (side chain hydroxyl group) by 1,3-cyclopentene dione. *R*-configured TX-2036 derivatives (TX-2043, TX-2030, and TX-2036) interacted with same amino acid residues (Lys[721], Thr[766]), whereas *S*-configured derivatives (TX-2044, TX-2031, TX-2037) interacted with various different amino acids of EGFR-tyk.
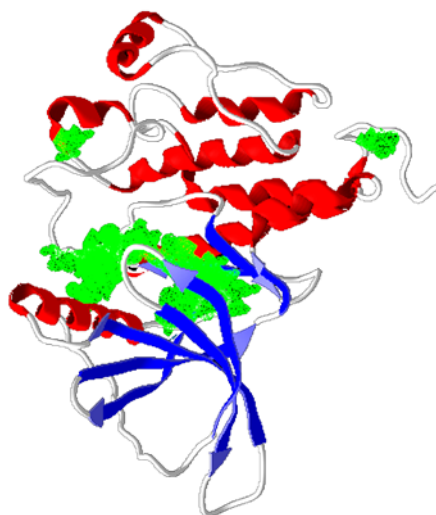
Figure 4-6.   Cavity analysis of tyrosine kinase domain of EGFR (EGFR-tyk).
The ligand-bindable pockets (green clouds) of EGFR-tyk were observed.
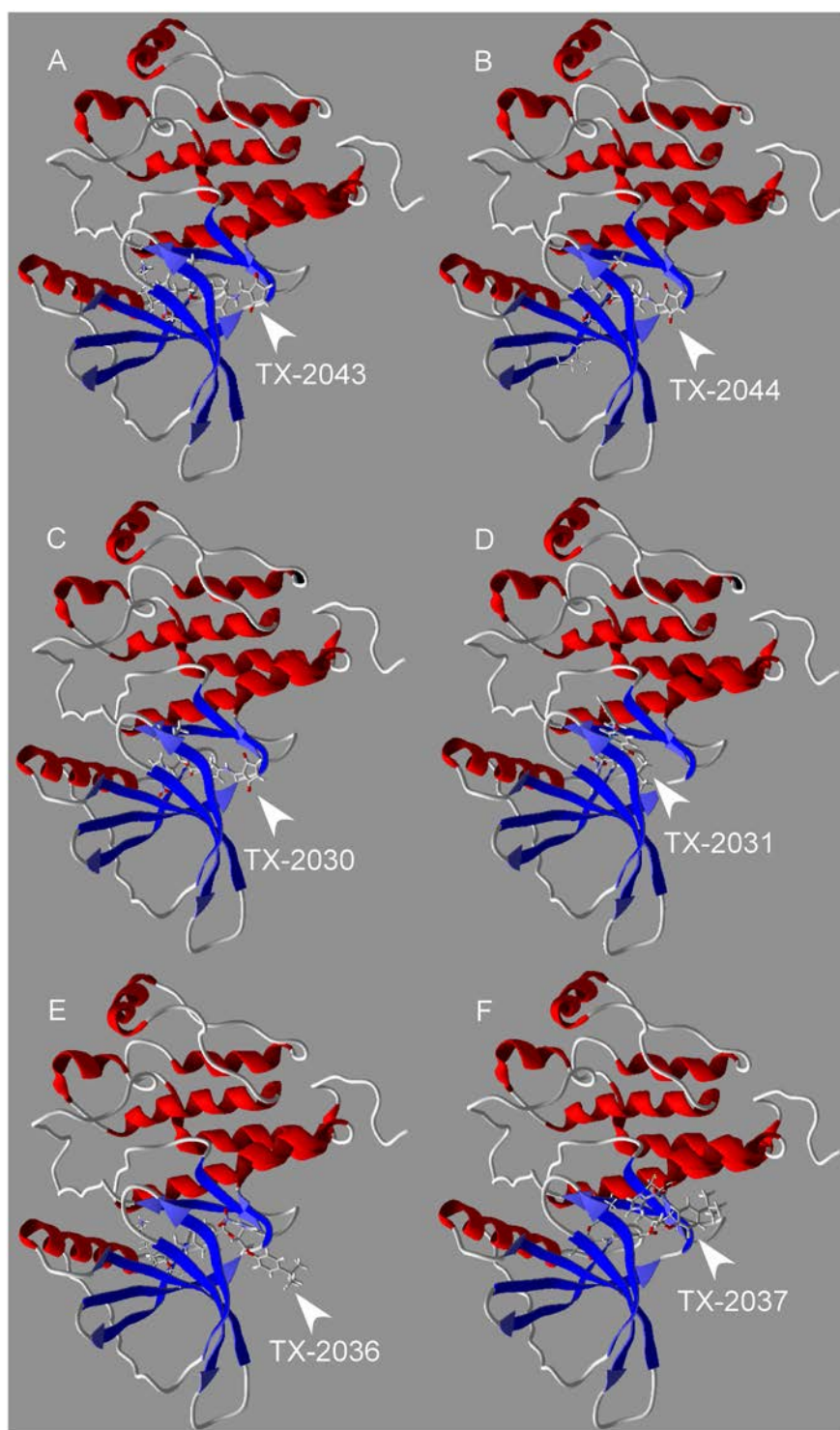
Figure 4-7.   Interactive analysis of TX-2036 derivatives with EGFR-tyk.
TX-2036 derivatives fitted into the cavity of the EGFR-tyk.
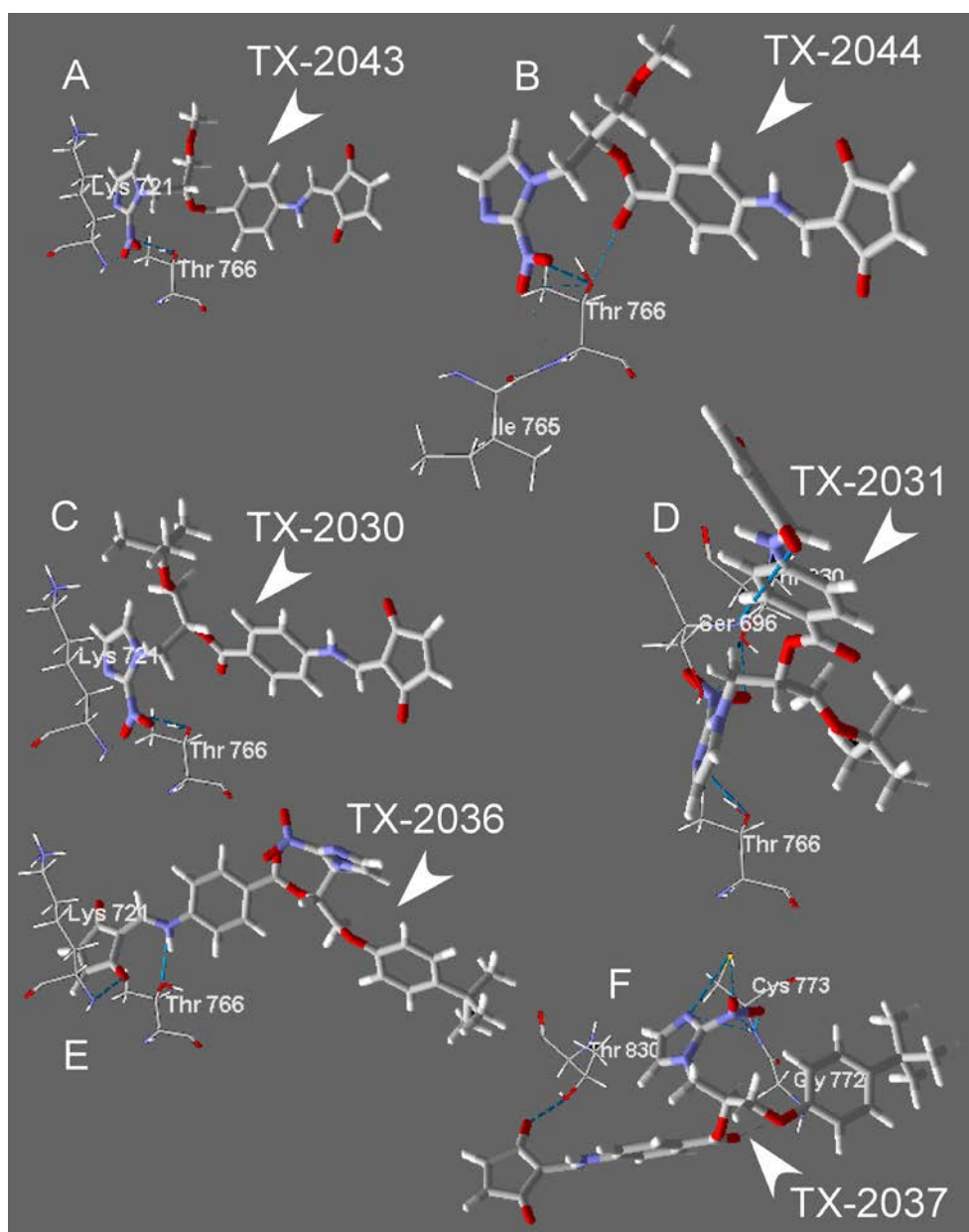
Figure 4-8.   Interactive profile of TX-2036 derivatives with EGFR-tyk.
R-configured TX-2036 derivatives (TX-2043, TX-2030, TX-2036) interacted same amino acid residues (Lys[721], Thr[766]).   *S*-configured TX-2044 (Ile[765], Thr[766]), TX-2031 (Ser[696], Thr[766], Thr[830]), TX-2037 (Gly[772], Cys[773], Thr[830]) reacted different amino acids from *R*-configured derivatives.

Table 4-III.   Interactive analysis of TX-2036 derivatives with EGFR-tyk.

TXs (chirality)	Interactive amino acids
TX-2043 (*R*)	Lys[721], Thr[766]
TX-2044 (*S*)	Ile[765], Thr[766]
TX-2030 (*R*)	Lys[721], Thr[766]
TX-2031 (*S*)	Ser[696], Thr[766], Thr[830]
TX-2036 (*R*)	Lys[721], Thr[766]
TX-2037 (*S*)	Gly[772], Cys[773], Thr[830]

52
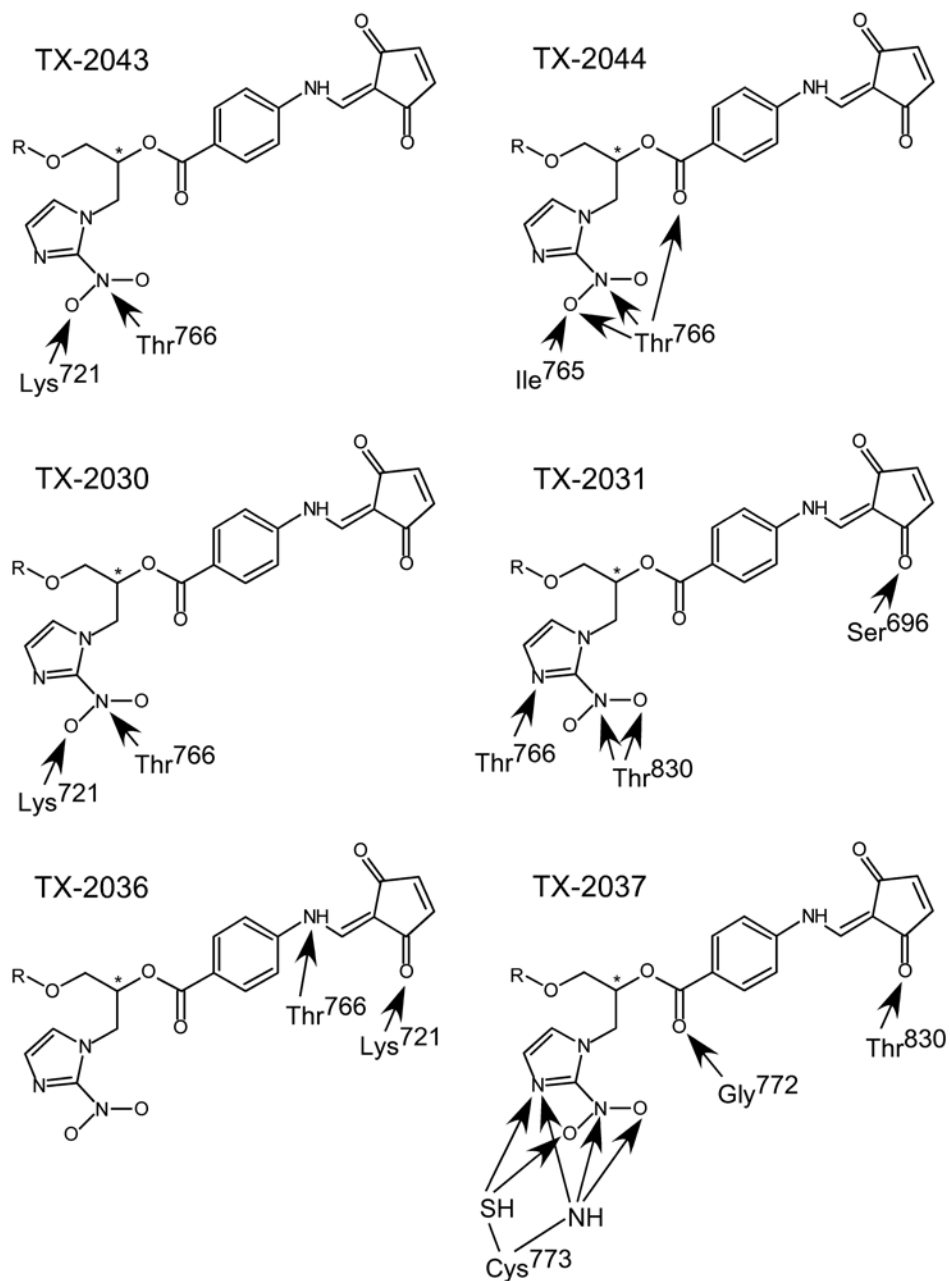
Figure 4-9.   Interactive profile between TX-2036 derivatives and EGFR-tyk.
Interacting amino acid residues of EGFR-tyk molecule were shown.

4-3-4. Discussion

TX-2036 possesses an asymmetric carbon and stereoisomers (*R*- and *S*-enantiomer) exist. Three dimensional aspects of TX-2036 derivatives should be analyzed to understand their molecular features. Inhibitory effect of *R*-configured TX-2036 derivatives on EGFR-tyk activity were stronger than those of *S*-configured derivatives. The EGFR-tyk inhibition was 10-fold different between *R*- and *S*-configured derivatives, and the IC_{50} values of *R*- and *S*-enantiomers were 1.8 − 21.3 µM and 18.4 − 213.0 µM, respectively. Spatial configuration of TX-2036 derivatives appeared to affect EGFR-tyk function. In molecular interactive simulation, *R*- and *S*-configured TX-2036 derivatives were bindable in EGFR-tyk. Molecular simulation confirmed that all *R*-configured derivatives (TX-2043, TX-2030, and TX-2036) interacted with Lys^{721} and Thr^{766} of EGFR-tyk. On the other hand, in the *S*-configured derivatives, interaction sites differed from *R*-configured derivatives. The interacting amino acid residues of EGFR-tyk differed for each *S*-derivative as follows: TX-2044 (Ile^{765} and Thr^{766}), TX-2031 (Ser^{696}, Thr^{766}, Thr^{830}), TX-2037 (Gly^{772}, Cys^{773}, Thr^{830}). No significant differences were observed in the positions at which *R*- and *S*-derivatives fit into the EGFR-tyk (Figure 4-7), however, the microenvironment of the interaction of *R*- and *S*-derivatives differed (Figure 4-8). By introducing an asymmetric center into the TX-2036 series, it became possible to modify their functions without changing the molecular bulkiness (*e.g.* molecular weight). TX-2036 has more bulky R-group (*p-tert*-butyl) than TX-2043 (methyl) and TX-2030 (*tert*-butyl), and interacted with the EGFR-tyk molecule at different region (*i.e.* 1,3-cyclopentene dione region) from other *R*-configured derivatives (Figure. 4-9). Bulkiness of TX-2036 R-group appears to produce the peculiar interactive manner with EGFR-tyk molecule.

Based on an analysis using the stereo-hydrophobicity parameter dGW (Ohkura K. *et al.* (1999), Zhu J.W. *et al.* (2000)), it was confirmed that a molecule with a bulky alkyl chain

((*tert*-butyl)$_2$-C$_2$H$_4$: dGW = -0.689kJ/mol) had lower hydrophobicity than that with a linear alkyl chain (C$_{10}$H$_{22}$: dGW = -0.708kJ/mol), and the degree of hydrophobicity may be adjusted by introducing a bulky region.   The absolute value of the difference in dGW value between the C$_{10}$H$_{22}$-straight alkyl molecule and the (*tert*-butyl)$_2$-C$_2$H$_4$ alkyl molecule was 0.019 kJ/mol. This difference was less than that corresponding to the difference (0.051 kJ/mol) of one carbone group (CH$_2$) obtained from a comparison of the dGW values of C$_{10}$-straight alkyl molecule (C$_{10}$H$_{22}$: dGW = -0.708kJ/mol) and C$_9$-straight alkyl molecule (C$_9$H$_{20}$: dGW = -0.657kJ/mol), and it was possible to finely adjust the degree of hydrophobicity.   That is, the degree of hydrophobicity can be adjusted by utilizing the difference in the three-dimensional structure, rather than simply changing the number of carbon atoms.

The bulkiness of a molecule appears to correlate with free energy, and if it has a bulky structure, the entropy of the molecule is expected to increase.   This example had been reported in consideration of Gibbs free energy in molecular design of other TX-derivatives (*e.g.* haloacetylcarbamoyl-2-nitroimidazole compounds) (Ohkura K. *et al.* (2007)).   It is described by the Gibbs free energy (G = U + pV - TS; where G: free energy, U: internal energy, p: pressure, V: volume, T: temperature, S: entropy).   Then the heat formation (total) energy is considered to be one of the indices for molecular bulkiness (volume), and the order of these TX-2036 derivatives was *p-tert*-butyl compounds (TX-2036, TX-2037: 4.7–18.6 kcal/mol) < methyl compounds (TX-2043, TX-2044: 8.8–22.9 kcal/mol) < *tert*-butyl compounds (TX-2030, TX-2031: 13.8–27.0 kcal/mol) (Ohkura K. *et al.* (2019)).   We considered that a *p-tert*-butyl moiety looks bulky but it is energetically compact for the molecular design.   Introduction of a compactly folded structure in molecular design appears to promote energy compactness.   Balance between various parameters, such as molecular compactness, stereo-hydrophobicity, and reactivity (stability), will be important for the development of efficient kinase (*e.g.* EGFR-tyk) control compounds.

Chapter 5.　Overview

In the molecular design and synthesis of TX-1123, TX-1877, and TX-2036 derivatives, each TX-series were examined individually.　However, looking back, TX-2036 had a structure that connected TX-1877 and TX-1123 (Figure 5-1).　Moreover, TX-1877 had an asymmetric carbon near the 2-nitroimidazole ring and had the property of producing stereoisomers.　There were four aromatic rings in TX-2036 molecule, and each ring formed four planes (green circles in Figure 5-2).　These four planes are linking, and generate many conformations by rotating and expanding, and contracting independently of each other.　This shows that infinite structures can be expressed in three-dimensional space by coordinating small molecules.
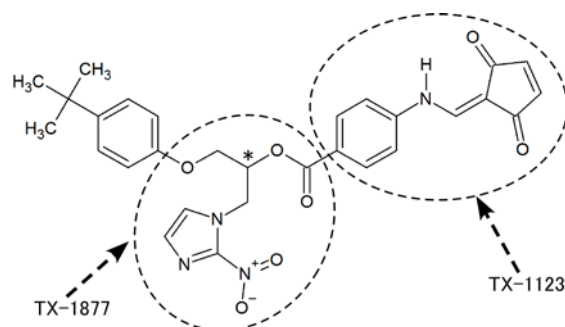
Figure 5-1.　Structure of TX-2036.
TX-2036 was constructed from TX-1123 and TX-1877 motif region.
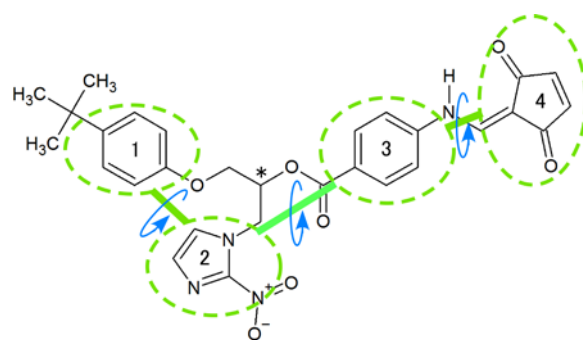
Figure 5-2.　Four planes of TX-2036.
The four planes (green circles) independently rotate and stretch.

56

The degree of hydrophobicity is an important factor for the expression of various biological activities including the interaction with biological membranes. In the structural changes on a rigid single plane, the pattern of hydrophobicity that occurs is limited, but the degree of hydrophobicity can vary greatly due to steric structural changes. In molecular design, the selection of the lead structure is important, but more importantly, consideration of structural flexibility, which produce the dynamic three-dimensional structure for creation of interactive ability with target molecules (*e.g.* COX, kinase, receptor molecule).

Acknowledgements

References

Abou-Bedair, F.A., Hori, H., Nagasawa, H., Uto, Y., Abu-Zeid, M., Inayama, S. (2002): Comparison of hypoxic cell radiosensitizers, KIN-804, KIN-844, KIN-806 and TX-1877, on brain and liver metabolizing capacities in mice bearing Ehrlich ascites carcinoma.
Biol Pharm Bull **25**, 591-596.

Baek, S.J., Eling, T.E. (2006): Changes in gene expression contribution to cancer prevention by COX inhibitors.
Prog Lipid Res **45**, 1-16.

Blume-Jensen, P., Hunter, T. (2001): Oncogenic kinase signalling.
Nature **411**, 355-365.

Brown, J.M.. Workman, P. (1980): Partition coefficient as a guide to the development of radiosensitizers which are less toxic than misonidazole.
Radiat Res **82**, 171-190.

Brunger, A.T., Nilges, M. (1993): Computational challenges for three dimensional structure determination by X-ray crystallography and solution NMR spectroscopy.
Quart Rev Biophys **26**, 49-125.

Chiba, A., Matsumura, K., Yamada, H., Inazu, T., Shimizu, T., Kusunoki, S., Kanazawa, I., Kobata, A., Endo, T. (1997): Structures of sialylated O-linked oligosaccharides of bovine peripheral nerve a-dystroglycan: The role of a novel O-mannosyl type oligosaccharide in the binding with laminin.
J Biol Chem **272**, 2156-2162.

Crofford, L.J. (1997): COX-1 and COX-2 tissue expression: implications and predictions.
J Rheumatol **24**, 15-19.

Fitzpatrick, F.A. (2004): Cyclooxygenase enzymes: regulation and function.
Curr Pharm Des **10**, 577-588.

Freire, E. (2008): Do enthalpy and entropy distinguish first in class from best in class?
Drug Discov Today **13**, 869-874.

Futaki, N., Takahashi, S., Yokoyama, M., Arai, I., Higuchi, S., Otomo, S. (1994): NS-398, a new anti-inflammatory agent, selectively inhibits prostaglandin G/H synthase/cyclooxygenase (COX-2) activity *in vitro*.
Prostaglandins **47**, 55-59.

Gazit, A., Yaish, P., Gilon, C., Levitzki, A. (1989): Tyrphostins I: synthesis and biological activity of protein tyrosine kinase inhibitors.
J Med Chem **32**, 2344-2352.

Gruner, S.M. (1994): X-Ray-detectors for macromolecular crystallography. *Curr Opin Struct Biol* **4**, 765-769.

Helliwell, J.R. (1992): Macromolecular crystallography with synchrotron radiation. Cambridge University Press, Cambridge.

Higashi, H., Suzuki-Takahashi, I., Saitoh, S., Segawa, K., Taya, Y., Okuyama. A., Nishimura, S., Kitagawa, M. (1996): Cyclin-dependent kinase-2 (Cdk2) forms an inactive complex with cyclin D1 since Cdk2 associated with cyclin D1 is not phosphorylated by Cdk7-cyclin-H.
Eur J Biochem **237**, 460-467.

Hori, H., Fujii, T., Kubo, A., Pan, N., Sako, S., Tada, C., Matsubara, T. (1994): KIH-201: a new enhancer of chemiluminescence in the luminol-hydrogen peroxide-peroxidase system characterized by a high-performance luminometer.
Anal Lett **27**, 1109-1122.

Hori, H., Maezawa, H., Iitaka, Y., Ohsaka, T., Shibata, T., Mori, T., Inayama, S. (1987): 2-Arylidene-4-cyclopentene-1,3-diones designed as non-nitro radiosensitizers and hypoxic cytotoxins.
Jpn J Cancer Res **78**, 1128-1133.

Hori, H., Nagasawa, H., Ishibashi, M., Uto, Y., Hirata, A., Saijo, K., Ohkura, K., Kirk, K.L., Uehara, Y. (2002): TX-1123: An antitumor 2-hydroxyarylidene-4-cyclopentene-1,3-dione as a protein tyrosine kinase inhibitor having low mitochondrial toxicity.
Bioorg Med Chem **10**, 3257-3265.

Hubbard, S.R., Till, J.H. (2000): Protein tyrosine kinase structure and function.
Annu Rev Biochem **69**, 373-398.

Idutsu, Y., Sasaki, A., Matsumura, S., Toshima, K. (2005): Molecular design, chemical synthesis, and evaluation of cytosine-carbohydrate hybrids for selective recognition of a single guanine bulged duplex DNA.
Bioorg Med Chem Lett **15**, 4332-4335.

Inayama, S., Mamoto, K., Shibata, T., Hirose, T. (1976): Structure and antitumor activity relationship of 2-arylidene-4-cyclopentene-1,3-diones and 2-arylideneindan-1,3-diones.
J Med Chem **19**, 433-436.

Jeffrey, P.D., Russo, A.A., Polyak, K., Gibbs, E., Hurwitz, J., Massague, J., Pavletich, N.P. (1995): Mechanism of CDK activation revealed by the structure of a cyclinA-CDK2 complex.
Nature **376**, 313-320.

Jin, C.Z., Nagasawa, H., Shimamura, M., Uto, Y., Inayama, S., Takeuchi, Y., Kirk, K.L., Hori, H. (2004): Angiogenesis inhibitor TX-1898: syntheses of the enantiomers of sterically diverse haloacetylcarbamoyl-2-nitroimidazole hypoxic cell radiosensitizers.
Bioorg Med Chem **12**, 4917-4927.

Kasai, S., Nagasawa, H., Kuwasaka, H., Oshodani, T., Nishioka, A., Ogawa, Y., Yoshida, S., Inayama, S., Inomata, T., Hori, H. (1998): TX-1877: design, synthesis, and biological activities as a BRM-functional hypoxic cell radiosensitizer.
Int J Radiat Oncol Biol Phys **42**, 799-802.

Kasai, S., Nagasawa, H., Yamashita, M., Masui, M., Kuwasaka, H., Oshodani, T., Uto, Y., Inomata, T., Oka, S., Inayama, S., Hori, H. (2001): New antimetastatic hypoxic cell radiosensitizers: design, synthesis, and biological activities of 2-nitroimidazole-acetamide, TX-1877, and its analogues.
Bioorg Med Chem **9**, 453-464.

Kawaguchi, Y., Tabata, A., Nagamune, H., Ohkura, K. (2013): Profiles of ILY, VLY and Sm-hPAF interaction with human CD59.
Anticancer Res **33**, 2901-2904.

Klebe, G. (2015): Applying thermodynamic profiling in lead finding and optimization.
Nat Rev Drug Discov **14**, 95-110.

Koike, H., Hori, H., Inayama, S., Terada, H. (1988): Effect of arylidene-cyclopentenedione radiosensitizers on ATP synthesis in mitochondria: Action as potent inhibitors of phosphate transport.
Biochem Biophys Res Commun **155**, 1066-1074.

Levitzki, A. (1990): Tyrphostins-potential antiproliferative agents and novel molecular tools.
Biochem Pharmacol **40**, 913-918.

Levitzki, A. (1992): Tyrphostins: tyrosine kinase blockers as novel antiproliferative agents and dissectors of signal transduction.
FASEB J **6**, 3275-3282.

Levitzki, A., Gazit, A. (1995): Tyrosine kinase inhibition: an approach to drug development.
Science **267**, 1782-1788.

Liu, L. (2015): Antibody glycosylation and its impact on the pharmacokinetics and pharmacodynamics of monoclonal antibodies and Fc-fusion proteins.
J Pharm Sci **104**, 1866-1884.

Mikata, Y., Shinohara, Y., Yoneda, K., Nakamura, Y., Esaki, K., Tanahashi, M., Brudzinska, I., Hirohara, S., Yokoyama, M., Mogami, K., Tanase, T., Kitayama, T., Takashiba, K., Nabeshima, K., Takagi, R., Takatani, M., Okamoto, T., Kinoshita, I., Doe, M., Hamazawa, A., Morita, M., Nishida, F., Sakakibara, T., Orvig, C., Yano, S. (2001): Sugar-pendant diamines.
J Org Chem **66**, 3783-3789.

Miyake, K., Shimada, M., Nishioka, M., Sugimoto, K., Batmunkh, E., Uto, Y., Nagasawa, H., Hori, H. (2008): The novel hypoxic cell radiosensitizer, TX-1877 has antitumor activity through suppression of angiogenesis and inhibits liver metastasis on xenograft model of pancreatic cancer.
Cancer Lett **272**, 325-235.

Murakami, Y., Fukazawa, H., Mizuno, S., Uehara, Y. (1994): Conversion of epidermal growth factor (EGF) into a stimulatory ligand for A431-cell growth by herbimycin A by decreasing the level of expression of EGF receptor.
Biochem J **301**, 57-62.

Nagasawa, H., Uto, Y., Kirk, K.L., Hori H. (2006): Design of Hypoxia-Targeting Drugs as New Cancer Chemotherapeutics.
Biol Pharm Bull **29**, 2335-2342.

Nakae, T., Uto, Y., Tanaka, M., Shibata, H., Nakata, E., Tominaga, M., Maezawa, H., Hashimoto, T., Kirk, K.L., Nagasawa, H., Hori, H. (2008): Design, synthesis, and radiosensitizing activities of sugar-hybrid hypoxic cell radiosensitizers.
Bioorg Med Chem **16**, 675-682.

Ohkura, K., Hori, H. (1999): Analysis of structure-permeability correlation of nitrophenol analogues in newborn rat abdominal skin using semiempirical molecular orbital calculation.
Bioorg Med Chem **7**, 309-314.

Ohkura, K., Hori, H. (2001): Modification of cell response to insulin by membrane-acting agents in rat white adipocytes: analysis of structural features by computational simulation.
Bioorg Med Chem **9**, 3023-3033.

Ohkura, K., Hori, H., Shinohara, Y. (2009): Role of C-terminal region of yeast ADP/ATP carrier 2 protein: dynamics of flexible C-terminal arm.
Anticancer Res **29**, 4897-4900.

Ohkura, K., Kawaguchi, Y., Tabata, A., Yamamoto, A., Shinohara, Y., Nagamune, H., Hori, H. (2012): Molecular profiles of cholesterol dependent cytolysin family-derived 11mer regions.
Anticancer Res **32**, 2343-2346.

Ohkura, K., Kawaguchi, Y., Tatematsu, Y., Uto, Y., Hori, H. (2016): An antitumor 2-hydroxyarylidene-4-cyclopentene-1,3-dione as a protein tyrosine kinase inhibitor: Interaction between TX-1123 derivatives and Src kinase.
Anticancer Res **36**, 3645-3649.

Ohkura, K., Sukeno, A., Nagamune, H., Kourai, H. (2005): Bridge-linked bis-quaternary ammonium anti-microbial agents: relationship between cytotoxicity and anti-bacterial activity of 5,5'-[2,2'-(tetramethylenedicarbonyldioxy)- diethyl] bis (3-alkyl-4-methylthiazonium iodide)s.
Bioorg Med Chem **13**, 2579-2587.

Ohkura, K., Sukeno, A., Yamamoto, K., Nagamune, H., Maeda, T., Kourai, H. (2003): Analysis of structural features of bis-quaternary ammonium antimicrobial agents 4,4'-(alpha,omega-polymethylenedithio) bis (1-alkylpyridinium iodide)s using computational simulation.
Bioorg Med Chem **17**, 5035-5043.

Ohkura, K., Tabata, A., Uto, Y., Hori, H. (2019): Correlation between radiosensitizing activity and the stereo-structure of the TX-2036 series of molecules. *Anticancer Res* **39**, 4479-4483.

Ohkura, K., Tatematsu, Y., Kawaguchi, Y., Uto, Y., Hori, H. (2017): Interactive analysis of TX-1123 with cyclo-oxygenase: Design of COX2 selective TX analogs.
Anticancer Res **37**, 3849-3854.

Ohkura, K., Uto, Y., Nagasawa, H., Hori, H. (2007): Effect of molecular chirality and side chain bulkiness on angiogenesis of haloacetylcarbamoyl-2-nitroimidazole compounds.
Anticancer Res **27**, 3693-3700.

Oshikawa, T., Okamoto, M., Ahmed, S.U., Furuichi, S., Tano, T., Sasai, A., Kan, S., Kasai, S., Uto, Y., Nagasawa, H., Hori, H., Sato, M. (2005): TX-1877, a bifunctional hypoxic cell radiosensitizer, enhances anticancer host response: immune cell migration and nitric oxide production.
Int J Cancer **116**, 571-578, 2005.

Otto, R., Brox, J., Trippel, S., Stei, M., Best, T., Wester, R. (2012): Single solvent molecules can affect the dynamics of substitution reactions.
Nature Chem 4, 534-538.

Palumbo, G.A., Yarom, N., Gazit, A., Sandalon, Z., Baniyash, M., Kleinberger-Doron, N., Levitzki, A., Ben-Yehuda, D. (1997): The tyrphostin AG17 induces apoptosis and inhibition of CDK2 activity in a lymphoma cell line that overexpresses BCL-2.
Cancer Res **57**, 2434-2439.

Pandey, S.K., Zheng, X., Morgan, J., Missert, J.R., Liu, T.H., Shibata, M., Bellnier, D.A., Oseroff, A.R., Henderson, B.W., Dougherty, T.J., Pandey, R.K. (2007): Purpurinimide carbohydrate conjugates: Effect of the position of the carbohydrate moiety in photosensitizing efficacy.
Mol Pharmaceutics **4**, 448-464.

Richardson, J.M., Morla, A.O., Wang, J.Y. (1987): Reduction in protein tyrosine phosphorylation during differentiation of human leukemia cell line K-562.
Cancer Res **47**, 4066-4470.

Rossmann, M.G., McKenna, R., Tong, L., Xia, D., Dai, J-B., Wu, H., Choi, H-K., Lynch, R.E. (1992): Molecular replacement real-space averaging.
J Appl Cryst **25**, 166-180.

Shibamoto, Y., Ono, K., Takahashi, M., Kano, E., Hori, H., Shibata, T., Inayama, S., Abe, M. (1986): An *in vitro* and *in vivo* screening system for new hypoxic cell radiosensitizers using EMT6 cells.
Jpn J Cancer Res **77**, 1027-1033.

Steinmeyer, J. (2000): Pharmacological basis for the therapy of pain and inflammation with nonsteroidal anti-inflammatory drugs.
Arthritis Res **2**, 379-385.

Suleyman, H., Demircan, B., Karagoz, Y. (2007): Anti-inflammatory and side-effects of cyclo-oxygenase inhibitors.
Pharmacol Rep **59**, 247-258.

Sylvaina, I., Zerroukia, R., Graneta, R., Huanga, Y.M., Lagorcea, J.F., Guillotona, M., Blaisb, J.C., Krausza, P. (2002): Synthesis and biological evaluation of thioglycosylated porphyrins for an application in photodynamic therapy.
Bioorg Med Chem **10**, 57-69.

Terada, H., Fukui, Y., Shinohara, Y., Ju-ichi, M. (1988): Unique action of a modified weakly acidic uncoupler without an acidic group, methylated SF6847, as an inhibitor of oxidative phosphorylation with no uncoupling activity: possible identity of uncoupler binding protein.
Biochim Biophys Acta **933**, 193-199.

Toshima, K., Okuno, Y., Matsumura, S. (2003): Glycidol-carbohydrate hybrids: a new family of DNA alkylating agents.
Bioorg Med Chem Lett **13**, 3281-3283.

Toshima, K., Okuno, Y., Nakajima, Y., Matsumura, S. (2002): Beta-carboline-carbohydrate hybrids: molecular design, chemical synthesis and evaluation of novel DNA photocleavers.
Bioorg Med Chem Lett **12**, 671-673.

Toshima, K., Ozawa, T., Kimura, T., Matsumura, S. (2004): The significant effect of the carbohydrate structures on the DNA photocleavage of the quinoxaline-carbohydrate hybrids.
Bioorg Med Chem Lett **14**, 2777-2779.

Ullrich, A., Schlessinger, J. (1990): Signal transduction by receptors with tyrosine kinase activity.
Cell **61**, 203-212.

Umezawa, H., Imoto, M., Sawa, T., Isshiki, K., Matsuda, N., Uchida, T., Iinuma, H., Hamada, M., Takeuchi, T. (1986): Studies on a new epidermal growth factor-receptor kinase inhibitor, erbstatin, produced by MH435-hF3.
J Antibiot **39**, 170-173.

Uto, Y., Nagasawa, H., Jin, C.Z., Nakayama, S., Tanaka, A., Kiyoi, S., Nakashima, H., Shimamura, M., Inayama, S., Fujiwara, T., Takeuchi, Y., Uehara, Y., Kirk, K.L., Nakata, E., Hori, H. (2008): Design of antiangiogenic hypoxic cell radiosensitizers: 2-nitroimidazoles containing a 2-aminomethylene-4-cyclopentene-1,3-dione moiety.
Bioorg Med Chem **16**, 6042-6053.

Vane, J.R., Bakhle, Y.S., Botting, R.M. (1998): Cyclooxygenases 1 and 2.
Annu Rev Pharmacol Toxicol **38**, 97-120.

Wang, X., Baek, S.J., Eling, T. (2011): COX inhibitors directly alter gene expression: Role in cancer prevention?
Cancer Metastasis Rev **30**, 641-657.

Watanabe, T., Tanigawa, T., Nadatani, Y., Otani, K., Machida, H., Okazaki, H., Yamagami, K., Watanabe, K., Tominaga, K., Fijiwara, Y., Arakawa, T. (2011): Mitochondrial disorders in NSAIDs-induced small bowel injury.
J Clin Biochem Nutr **48**, 117-121.

Yaish, P., Gazit, A., Gilon, C., Levitzki, A. (1988): Blocking of EGF dependent cell proliferation by EGF receptor kinase inhibitors.
Science **242**, 933-935.

Yoshida, A., Kobayashi, K., Manya, H., Taniguchi K., Kano, H., Mizuno, M., Inazu, T., Mitsuhashi, H., Takahashi, S., Takeuchi, M., Hermann, R., Straub, V., Talim, B., Voit, T., Topaloglu, H., Toda, T., Endo, T. (2001): Muscular dystrophy and neuronal migration disorder caused mutations in a glycosyltransferase, POMGnT1.
Dev Cell **1**, 717-724.

Yoshino, T., Kimoto, A., Kobayashi, S., Noguchi, M., Fukunaga, M., Hayashi, A., Miyata, K., Sasamata, M. (2005): Pharmacological profile of celecoxib, a specific cyclo-oxygenase-2 inhibitor.
Arzneimittelforschung **55**, 394-402.

Zhu, J.W., Nagasawa, H., Nagura, F., Mohamad, S.B., Uto, Y., Ohkura, K., Hori, H. (2000): Elucidation of strict structural requirements of brefeldin A as an inducer of differentiation and apoptosis.
Bioorg Med Chem **8**, 455-463.

List of Publications

An Antitumor 2-Hydroxyarylidene-4-cyclopentene-1,3-Dione as a Protein Tyrosine Kinase Inhibitor: Interaction Between TX-1123 Derivatives and Src Kinase.
Ohkura, K., Kawaguchi, Y., Tatematsu, Y., Uto, Y., Hori, H.
Anticancer Res **36**, 3645-3649, 2016.

Interactive Analysis of TX-1123 with Cyclo-oxygenase: Design of COX2 Selective TX Analogs.
Ohkura, K., Tatematsu, Y., Kawaguchi, Y., Uto, Y., Hori, H.
Anticancer Res **37**, 3849-3854, 2017.

Structure-associated Functional Control of TX-1877 Series by Glyco-conjugation.
Ohkura, K., Kawaguchi, Y., Tatematsu, Y., Tabata, A., Uto, Y., Hori, H.
Anticancer Res **38**, 4241-4245, 2018.

Correlation between Radiosensitizing Activity and the Stereo-structure of the TX-2036 Series of Molecules.
Ohkura, K., Tabata, A., Uto, Y., Hori, H.
Anticancer Res **39**, 4479-4483, 2019.